ISSN 1580-2949
UDK 669+666+678+53 MTAEC9, 42(5)189–233(2008)

MATER. TEHNOL.	LETNIK VOLUME 42	ŠTEV. NO. 5	STR. P. 189–233	LJUBLJANA SLOVENIJA	SEP.–OCT. 2008

VSEBINA – CONTENTS

IZVIRNI ZNANSTVENI ČLANKI – ORIGINAL SCIENTIFIC ARTICLES

STROKOVNI ČLANKI – PROFESSIONAL ARTICLES

UDK 669.715:539.42
Original scientific article/Izvirni znanstveni članek

ISSN 1580-2949
MTAEC9, 42(5)191(2008)

THE EFFECT OF COMPOSITIONAL VARIATIONS ON THE FRACTURE TOUGHNESS OF 7000 Al-ALLOYS

VPLIV SPREMEMB V SESTAVI NA ŽILAVOST LOMA ALUMINIJEVE ZLITINE VRSTE 7000

Maja Vratnica[1], Zorica Cvijović[2], Nenad Radović[2]

[1] Faculty of Metallurgy and Technology, University of Montenegro, 81000 Podgorica, Cetinjski put b. b., Montenegro
[2] Faculty of Technology and Metallurgy, University of Belgrade, 11000 Belgrade, Karnegijeva 4, Serbia
majav@cg.ac.yu

Prejem rokopisa – received: 2008-02-12; sprejem za objavo – accepted for publication: 2008-04-03

To provide an understanding of how compositional variations affect the microstructural parameters associated with coarse intermetallic (IM) particles and the fracture toughness in AA 7000 aluminum forgings, a microstructural and fractographic analysis as well as mechanical tests were carried out on three industrially produced Al-Zn-Mg-Cu alloys with different contents of impurities (Fe+Si). Light optical microscopy and image analysis were used to assess the volume fraction, size and distribution of all the soluble and insoluble coarse (> 0.1 μm) IM particles identified in the corresponding R-C and L-R planes for T73-type heat treatments by selective etching and energy-dispersive X-ray spectroscopy. These quantitative data were correlated with the plain-strain fracture toughness, K_{IC}, with the results being used to produce useful information on alloy design and thermomechanical processing via microstructural control. The scanning electron microscope observation of fracture surface features and an estimation of the area fractions of different fracture modes in the plastic zone segments of a test specimen showed that multiple failure mechanisms occurred with coarse voiding at the intermetallics becoming more important as the fraction of coarse IM particles increases. A quantitative assessment of the relevant microstructural and fractographic parameters will be utilized for developing and verifying a multiple micromechanisms-based model for fracture toughness.

Key words : 7000 Al- alloys, chemical composition, microstructure, fracture toughness

S ciljem, da se ugotovi, kako spremembe v sestavi vplivajo na parametre mikrostrukture, odvisne od velikih delcev intermetalnih spojin (IM), in na žilavost loma v izkovkih iz zlitine AA 7000, so bile izvršene mikrostrukturne, mikrofraktografske in mehanske preiskave pri treh industrijskih zlitinah Al-Zn-Mg-Cu z različno vsebnostjo nečistoč (Fe + Si). Optična mikroskopija in analiza slike sta bili uporabljeni za določitev volumenskega deleža, velikosti in porazdelitve topnih in netopnih velikih (>0,1 μm) IM-zrn v ustreznih R-C- in L-R-ploskvah po toplotni obdelavi T73 s selektivnim jedkanjem in z disperzivno spektroskopijo rentgenskih žarkov. Ti kvantititivni podatki so bili korelirani z žilavostjo loma K_{IC}, dobljeni pa so bili tudi podatki, ki so koristna informacija za načrtovanje zlitin in termomehansko obdelavo s kontrolo mikrostrukture. Analiza prelomnih površin z vrstičnim mikroskopom in določitev površine različnih deležev preloma v plastični zoni preizkušancev je pokazala več vrst mehanizmov preloma in nastanek tem več velikih jamic ob IM-zrnih, čim večji je bil delež teh velikih zrn. Kvantitativna ocena relevantnih mikrostrukturnih in mikrofraktografskih parametrov bo uporabljena za razvoj in za verifikacijo modela žilavosti loma na podlagi več mahanizmov preloma.

Ključne besede: aluminijeva 7000 zlitina, kemična sestava, mikrostruktura, žilavost loma

1 INTRODUCTION

High-strength aluminum alloys of the AA 7000 (Al-Zn-Mg-Cu) series are widely used for structural applications due to their good combination of specific strength and fracture toughness[1]. However, the critical fracture toughness properties, especially in the short transverse direction, may be seen as questionable, since the fracture resistance is influenced by a number of parameters, including a range of microstructural features that are controlled by the chemistry and processing[1,2,3,4]. Furthermore, the microstructural anisotropy associated with wrought materials may influence the failure mode depending on the load and crack orientation[2].

It is now recognized that the coarse particles of intermetallic (IM) phases are generally detrimental to the fracture properties. This is associated with the fact that although the fracture processes in precipitation-hardened AA 7000 alloy products involve multiple micromechanisms, the decohesion and fracture of these particles, which are brittle and have weak interface bonding, is the first step in a sequence of events that lead to the overall material fracture[1,2,5]. The remaining fracture path is partitioned between intergranular fracture and micro-void-induced transgranular fracture.

The undesirable coarse particles with sizes in the range of 1 μm to 20 μm are IM phases of two types: (a) insoluble Fe- and Si-bearing phases formed during the solidification process, and (b) normally soluble phases containing alloying elements that do not completely dissolve during the homogenization and solution treatment[1]. In order to improve the toughness, it is necessary to achieve the lowest levels of coarse IM particles. The removal of excess amounts of the soluble particles is possible by controlling all the stages of processing. But, the limits on the reduction of the Fe and Si impurities are set by the cost and the availability of high-purity materials. Consequently, these impurities are always present in commercial alloys. They react with Al and alloying elements such as Mg and Cu to form a large

number of phases[6]. In addition, these alloys contain Mn and Cr, which may also be present in the form of coarse IM particles, since they combine with Fe, Si and Al.

Therefore, it is of interest to predict the variation in the fracture properties as a function of the microstructural parameters, such as the volume fraction of coarse IM particles, their size and their spatial distribution. However, most of the available information is concerned with the properties of wrought alloys. Systematic and in-depth quantitative microstructural and fractographic examinations of commercial AA 7000 alloys in the form of thick plates cut out from forgings have not been widely conducted. It is the purpose of this contribution to report on a microstructural and fractographic investigation of the effect of compositional variations on the attributes associated with coarse IM particles and the fracture toughness of modern AA 7000 alloy forgings (the high-zinc variant) in the over-aged condition as a function of test orientation. The failure mechanisms are identified and the individual contributions to the overall fracture are quantitatively assessed. The data are then used to obtain a relationship between the microstructural parameters and the plane-strain fracture toughness, with the results being utilized for the modeling of toughness.

2 EXPERIMENTAL

Three industrial alloys with Zn, Mg, and Cu levels broadly in the range of the AA 7049 composition were received in the form of hot-forged ≈50-mm-thick pancake-type plates. The chemical composition of each alloy is given in **Table 1**. The amounts of alloying elements are very near to the nominal ones. The only difference in composition between the alloys is the total (Fe+Si) content, which increases gradually from alloy 1 through alloy 3. **Figure 1** shows the cutting of the tests specimens from the received plates.

All three alloys were solution treated at 460 °C for 1 h, water-quenched, and aged to a T73 temper. The two-step T73 over-aged treatment consisted of the aging of the specimens for 5 h at 100 °C and 5 h at 160 °C. Light optical microscopy (LOM) and image analyses were used to characterize the microstructure of the as-heat-treated plates. Metallographic sections were taken from the corresponding R-C and L-R planes. The specimens were then prepared using standard metallographic techniques. A selective etching and energy-dispersive X-ray spectroscopy (EDS) analysis on a scanning electron microscope (SEM) were used to identify the IM phases present. The volume fraction of all the soluble and insoluble coarse IM particles, V_V, their size expressed by the average intercept length, L, and the mean free path, λ, characterizing the space distribution were assessed with the line-intercept method. The measurements were carried out on 500 uniformly sampled microstructural frames at a magnification of 1000 times. Plane-strain fracture-toughness tests were performed in accordance with ASTM E399 on the specimens of the corresponding R-C and L-R orientations, i.e., on the single-edge-notched three-point bending specimens (SEB) of R-C orientation and the compact-tension (CT) specimens of L-R orientation. The specimens were fatigue pre-cracked according to the ASTM standard specifications. In all cases, three specimens were tested. The K_{IC} values for the R-C orientation specimens were obtained from the J-integral data. J_{IC} was evaluated with the unloading compliance technique, with a single specimen for each J_{IC} result. The J-integral and the crack growth, Δa, were calculated in accordance with ASTM E1152 and ASTM E813. On a broken specimen an SEM fractographic examination was performed to explain the fracture mechanism. The fracture surface morphology was investigated in the central region of the plastic zone ahead of the fatigue pre-crack. The area fraction of the microvoid-induced transgranular fracture regions, A_{At}, the intergranular fracture regions, A_{Ai}, and the coarse IM particles, A_{Ap}, were estimated. The area measurements were performed on SEM fractographs by tracing the areas on a digitizing

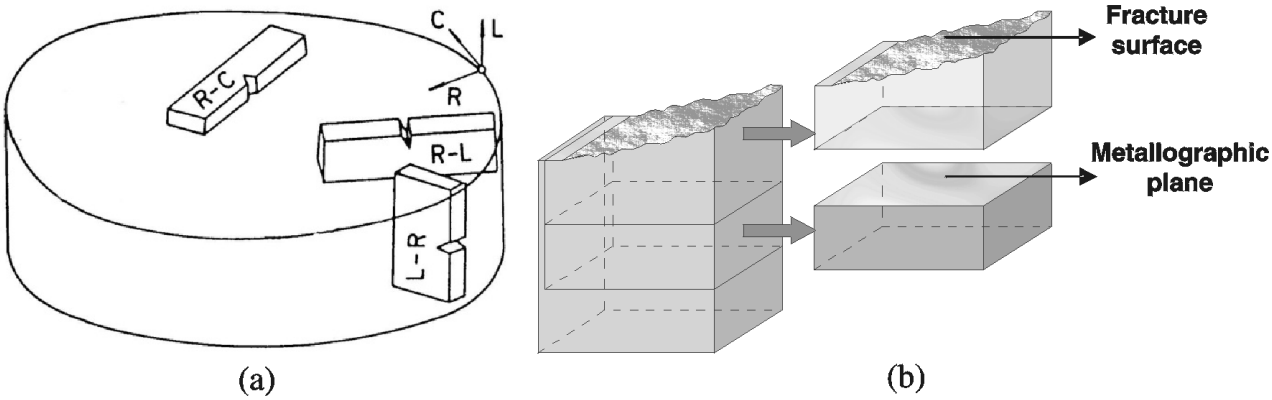

Figure 1: (a) Schematic illustration of the specimen orientations used for the fracture-toughness tests (L-longitudinal direction, C-circumferential or tangential direction, R-radial direction) and (b) locations of the metallographic planes for the microstructural analysis (b)
Slika 1: (a) Shema orientacije vzorcev, uporabljenih za preizkuse žilavosti loma (L-vzolžna smer, C tangencialna smer, R – radialna smer) in (b) mesto odvzema vorcev za mikrostrukturno analizo

tablet. These measurements provided the data to quantify the contributions of the different fracture micromechanisms to the plane-strain fracture-initiation process as a function of the purity degree and the specimen orientation.

3 RESULTS AND DISCUSSION

3.1 Analysis of the microstructural data

Typical microstructures of simple uniaxially forged material after the full heat treatment are illustrated in **Figure 2**.

All the forgings show a deformed dendrite cell structure with coarse IM particles having an average size of 1.27–2.43 μm. As expected, relatively coarse and closely spaced precipitates, mostly situated on the grain boundary surrounded by the precipitate-free zones (PFZs), were also observed (**Figure 2a**). The TEM characterization of the precipitation in AA 7000 alloys by previous authors[1,2] indicates that these particles are variants of the η-$Mg(Cu,Al,Zn)_2$ phase. In the Al-rich matrix there was a dense population of uniformly distributed dispersoids[1,2,4] and fine precipitates of the η and η' phases[1,2] that contributed to the precipitation hardening. On the other hand, the coarse IM particles are inhomogeneously distributed and aligned in the direction of the prevailing deformation, as observed on the metallographic plane of L-R orientation (**Figure 2b**). The micrographs also illustrate the IM particles that are irregularly shaped and of different types (**Figures 2c and d**). The combined use of the metallographic and EDS analyses indicates that these particles are of the following types: (a) soluble $Mg(Cu,Al,Zn)_2$, S-$CuMgAl_2$, and, most often observed, Mg_2Si, (b) the Fe-bearing phases Al_7Cu_2Fe, $(Cu,Fe,Mn)Al_3$ and a very little of $(Cu,Fe,Mn)Al_6$, (c) the Cr-bearing phase $(Cu,Fe,Mn,Cr)Al_7$, and (d) another type of Si-containing phases $(Fe,Cr,Mn,Cu)_3SiAl_{12}$.

The identified phases were found in all three alloys; however, variations in the composition caused large changes in their fraction and their morphological characteristics. This observation was also supported by the image analyses. As can be seen from the data presented in **Table 2**, the alloy 3 had the highest percentage of

Table 1: Chemical composition of the investigated alloys (in mass fractions, *w*/%)
Tabela 1: Kemična sestava raziskanih zlitin (v masnih deležih, *w*/%)

Alloy	Elements										
	Zn	Mg	Cu	Mn	Cr	Zr	Ti	V	B	Fe	Si
1	7.45	2.47	1.53	0.25	0.17	0.15	0.015	0.003	0.003	0.12	0.11
2	7.30	2.26	1.55	0.29	0.18	0.13	0.015	0.007	0.003	0.16	0.09
3	7.65	2.26	1.55	0.25	0.18	0.11	0.017	0.005	0.003	0.26	0.11

Table 2: Results of the image analysis and the plane-strain fracture-toughness tests
Tabela 2: Razultati analize slike in določitve žilavosti loma

Alloy	Plane	K_{IC}/(MPa·m$^{1/2}$)	A_A*		IM phase characteristics			
					Type	V_V, φ/%	L/μm	λ/μm
1	R-C	45.50	ND***		$MgZn_2$+S	0.159	1.63	1024.8
					Fe-rich**	0.227	2.00	883.5
					Mg_2Si	0.125	1.74	1394.1
	L-R	43.16	P	0.152	$MgZn_2$+S	0.147	1.56	1054.7
			I	0.278	Fe-rich**	0.236	2.08	878.0
			T	0.570	Mg_2Si	0.144	1.94	1350.0
2	R-C	42.63	ND***		$MgZn_2$+S	0.048	1.29	2685.6
					Fe-rich**	0.357	1.99	557.0
					Mg_2Si	0.094	1.70	1806.7
	L-R	40.96	P	0.299	$MgZn_2$+S	0.095	1.27	1333.8
			I	0.304	Fe-rich**	0.440	2.06	465.5
			T	0.397	Mg_2Si	0.134	1.92	1425.1
3	R-C	40.53	ND***		$MgZn_2$+S	0.119	1.63	1363.4
					Fe-rich**	0.590	2.43	409.8
					Mg_2Si	0.147	1.95	1318.7
	L-R	37.67	P	0.378	$MgZn_2$+S	0.046	1.38	3031.4
			I	0.287	Fe-rich**	0.532	2.37	444.3
			T	0.335	Mg_2Si	0.146	2.09	1434.8

* Area fractions of microvoid-induced transgranular fracture regions (t), intergranular fracture region (i), and coarse constituent particles (p); ** Fe-rich phases = Al_7Cu_2Fe + $(Cu,Fe,Mn)Al_3$ + $(Cu,Fe,Mn)Al_6$ + $(Cu,Fe,Mn,Cr)Al_7$ + $(Fe,Cr,Mn,Cu)_3SiAl_{12}$; *** ND = not determined
* delež površine mikrojamičastega transkristalnega preloma (t), interkristalen prelom (i) in velikih IM- zrn (p); ** Z Fe bogate faze = Al_7Cu_2Fe + $(Cu,Fe,Mn)Al_3$ + $(Cu,Fe,Mn)Al_6$ + $(Cu,Fe,Mn,Cr)Al_7$ + $(Fe,Cr,Mn,Cu)_3SiAl_{12}$; *** ND = ni določeno

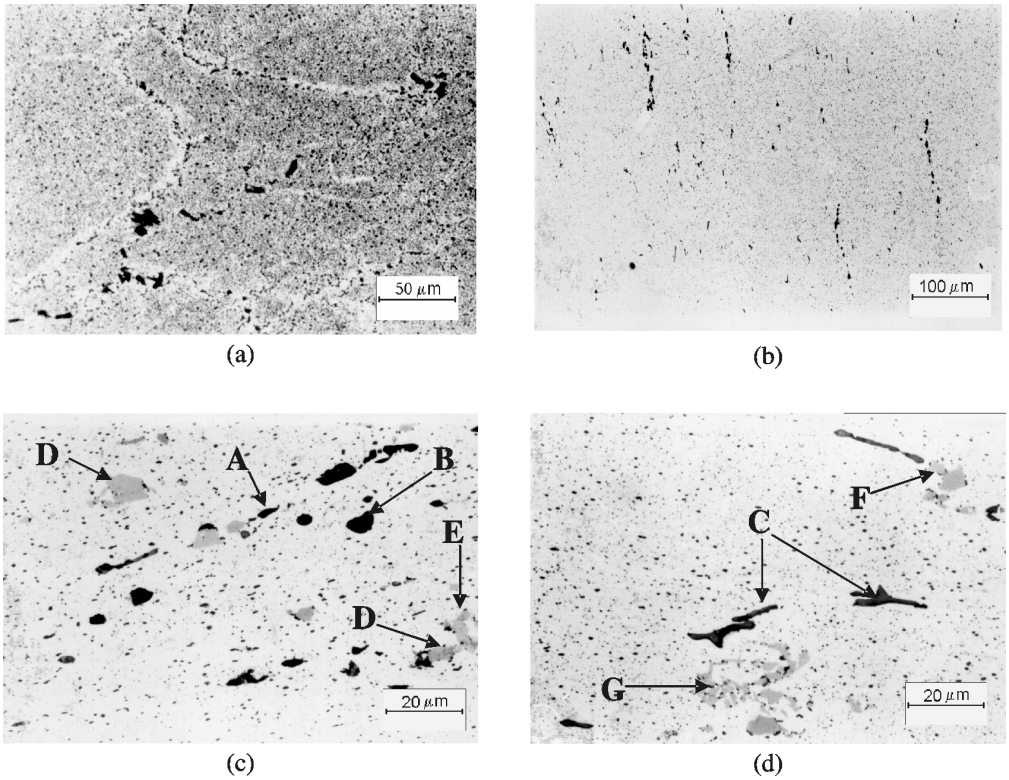

Figure 2: Optical microstructures of the over-aged alloy 3 (a),(c),(d) and alloy 1 (b) observed in R-C (a),(c) and L-R planes (b),(d) etched in 10 % H_3PO_4 at 50 °C for 5 min (a) and Keller's reagent at 20 °C for 5 s (b), (c), (d). Type of phases: A = $Mg(Cu,Al,Zn)_2$, B = S-$CuMgAl_2$, C = Mg_2Si, D = $(Cu,Fe,Mn)Al_3$ or $(Cu,Fe,Mn)Al_6$, E = Al_7Cu_2Fe, F = $(Cu,Fe,Mn,Cr)Al_7$, G = $(Fe,Cr,Mn,Cu)_3SiAl_{12}$.

Slika 2: Optična slika prestarane zlitine 3 (a), (b), (c) in (d) in zlitine 1 (b) v ploskvah R-C (a) in (c) ter L-R v ploskvah (b) in (d), jedkano v 10 % HPO_4 5 min (a) in s Keller reagentom 5 s pri 20 °C (b), (c) in (d). Vrste faz: A – $Mg(Cu,Al,Zn)_2$, B – S-$CuMgAl_2$, C – Mg_2Si, D – $(Cu,Fe,Mn)Al_3$ ali(Cu, Fe,Mn) Al_6, E – Al_7Cu_2Fe, F – $Cu,Fe,Mn,Cr)Al_7$, G – $Fe,Cr,Mn,Cu)_3SiAl_{12}$

coarse particles, with an average of volume fraction of 0.79 %, while the alloys 1 and 2 had a similar volume fraction, varying between about 0.52 % and 0.58 %. The significant increase in the amount of coarse particles, serving as the crack-initiation sites, is a direct consequence of an increase in the total (Fe+Si) content. For all the alloys, i.e., the volume fraction of phases containing Al, Mg, Cu, and Zn ($Mg(Cu,Al,Zn)_2$ and S-$CuMgAl_2$) is lower than ≈ 0.15 %. Note also that, since the Si content is practically unchanged from one alloy to the other, the volume fraction of Mg_2Si particles is constant. This implies that the Fe content plays an important role in the formation of coarse particles. The volume fraction of grey particles (Fe-containing phases) increases almost linearly with the increase in the Fe content. As a result, the coarse particles are distributed over shorter distances. These features can provide planes of easy crack growth, thereby reducing the deformation capacity of the matrix.

3.2 Toughness behavior

Table 2 shows how reducing the total (Fe+Si) content and thereby removing most of the coarse IM particles improves K_{IC}. As expected, the toughness was the highest for the alloy 1, with the lowest (Fe+Si) content of the mass fraction (w) 0.23 %. By increasing the impurity level from 0.23 % to 0.25 % and in turn the volume fraction of the Fe- and Si-containing particles from the volume fraction (φ) 0.380 % to 0.574 %, the K_{IC} value in the R-C orientation decreased by approximately by 6.5 %. Since in alloy 2 the Si content is w = 0.02 % and lower than that in the alloy 1, it is concluded that large variations in the amount of coarse particles and the fracture toughness can occur with a relatively small change in the Fe content. The toughness decreased further when going to a purity of w = 0.37 %. The drop in the fracture toughness, due to the presence of undesirable particles – φ = 0.298 % greater than in the microstructure of alloy 1 – is almost of 11 %.

The trend is similar for the L-R orientation. Although the amount of damaged particles has the greatest influence, a more probable explanation for the toughness degradation found in this work may be based on the synergistic effect of the coarse particles' volume fraction, their sizes and spacing. Namely, as the (Fe+Si) content increases the particle size increases, while the mean free path decreases, with a concomitant decrease in toughness. Thus, although the average particle size vary between 1.70 μm and 2.08 μm for the alloys 1 and 2, no distinct variation of the Fe-containing particle size with the orientation of the metallographic plane were

observed, whereas for the alloy 3 the particle size seemed to vary from 1.95 μm to 2.43 μm, with only minor differences between the R-C and L-R orientation planes. It should be noted that the Fe-containing particles were larger than those of the Mg_2Si phase and hence, more detrimental to K_{IC}, although a contribution from the other phases particles cannot be ruled out. Namely, larger particles are cracked more often. Also, the particles aligned in the loading direction are more prone to this type of damage. Therefore, the distribution of coarse particles is of particular importance. The metallographic examination showed that the spacing of the weak paths is also affected (at least for the R-C orientation plane). Decreasing the amount of particles leads to an increase in the mean interparticle distances. The λ value increases by 60 % to 80 %, going from alloy 3 to alloy 1, causing the absence of most particle stringers and decreasing the extent of coarse voiding with the IM particles. The comparison of the R-C and L-R orientations indicates that for a given degree of purity, the fracture toughness is different for a different direction of testing. All three alloys showed a higher toughness for the R-C-orientation specimens, as compared to that for the L-R orientation. This toughness anisotropy is particularly notable for alloy 3, with the highest (Fe+Si) content. The K_{IC} value in the R-C direction is higher by 7 % than the short-transverse value. This is primarily attributed to the anisotropic orientations of the coarse IM particles. This is consistent with the previously reported results[1,5] and indicates that the alignment of these particles seriously reduces K_{IC} and that it is even more efficient than the other possible paths of weakness, e.g., the grain boundaries with stringers of precipitates. Since coarse particles are brittle and fracture or separate from the matrix when the local strain exceeds a critical value, they provide preferential crack paths ahead of a crack at a high stress intensity. When such a stress intensity is applied, the presence of these preferential crack paths decreases the energy needed for the crack propagation. Hence, the toughness degradation can be attributed to an acceleration of the crack initiation and growth by the damaged particles.

The relative contributions of the different fracture modes to the plain-strain fracture initiation process (and, therefore, to K_{IC}) were determined from the fracture surfaces of the failed toughness specimens. SEM observations of the fracture surfaces revealed the multimechanism of the fracture process as a competition between coarse voiding at the IM particles and transgranular/intergranular failure. The controlling mechanism varies with the alloy purity, with the combination of transgranular/intergranular shearing dominating in alloy 1 (**Figure 3a**), and the coarse voiding becoming progressively more important as the (Fe+Si) content increases (**Figure 3b**).

The transgranular microvoid-induced fracture generated with the formation of voids around the matrix precipitates was observed in all cases. The shear planes

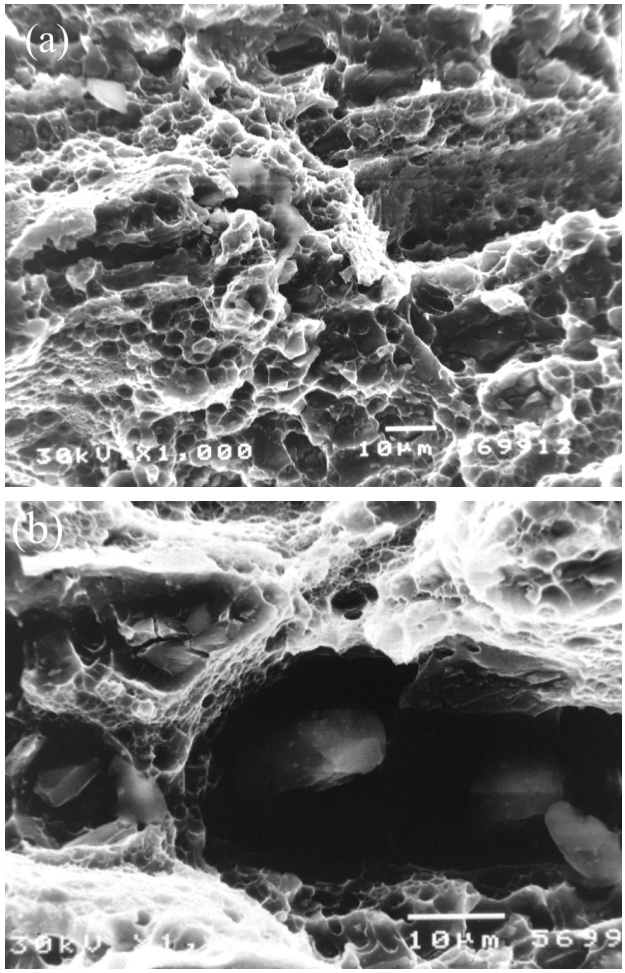

Figure 3: SEM micrographs showing the R-C fracture plane of alloy 1 (a) and the L-R fracture plane of alloy 3 (b).
Slika 3: SEM-posnetek preloma v R-C-ploskvi pri zlitini 1 (a) in L-R-preloma zlitine 3 (b)

were covered with fine dimples, commonly associated with very fine particles. Many extremely fine dimples, representing areas of extensive deformation that preceded the ductile fracture, were observed on the walls of very large dimples associated with the aggregates of mostly fractured IM particles. Places called ridges, where the crack had changed its direction of propagation, could also be identified. A higher magnification examination showed that they appear to be formed on the grain boundaries. Flat intergranular areas were characterized by a fine population of shallow dimples and coarse grain-boundary precipitates on some of them. The presence of the ridges suggests a competition between intergranular and transgranular shear-fracture mechanisms, although a greater extent of grain-boundary failure has not been observed.

In spite of the general similarity of the fracture surfaces for the alloy 1 through alloy 3, significant differences were also observed. The crack-propagation modes and the toughness levels are dependent on the extent of the primary void growth prior to the outset of

the secondary failure mode (i.e., intergranular and transgranular shear crack growth) and the intervoids linking. Since the primary voids initiate at coarse IM particles, it may be expected that an increase in the (Fe+Si) level, which in turn increases the amount of these particles, leads to an increased number of fractured particles, and therefore, a smaller extent of intergranular/transgranular shear fracture. **Figure 2b** illustrates this point very clearly, and it is also confirmed by the quantitative data in **Table 2**. The area fraction, A_{At}, of the microvoid-induced transgranular fracture decreases systematically with an increase in the volume fraction of the Fe- and Si-containing particles, while the area fraction, A_{Ap}, of the coarse IM particles on the fracture surface increases, leading to a decrease in the fracture toughness.

4 CONCLUSIONS

Quantitative microstructural and fractographical data showed that the coarse Fe- and S-containing particles had a very detrimental effect on the fracture toughness of over-aged Al-Zn-Mg-Cu forgings. The drop in K_{IC} was consistent with a change in the dominant failure mechanism, from intergranular/transgranular shear to extensive coarse void growth as the (Fe+Si) content increases from w = 0.23 to 0.37 %. This effect was attributed to the amount, size and spatial arrangement of the coarse IM particles and demonstrates the orientation dependence of the fracture toughness and the morphological anisotropy of the microstructure.

5 REFERENCES

[1] N. U. Deshpande, A. M. Gokhale, D. K. Denzer, John Liu, Metallurgical Materials Transactions A, 29A (**1998**) 4, 1191

[2] B. Morere, J.-C. Ehrstrom, P. J. Gregson, I. Sinclar, Metallurgical Materials Transactions A, 31A (**2000**) 10, 2503

[3] N. Kamp, I. Sinclair, M. J. Starink, Metallurgical Materials Transactions A, 33A (**2002**) 4, 1125

[4] R. C. Dorward, D. J. Beerntseen, Metallurgical Materials Transactions A, 26A (**1995**) 9, 2481

[5] A. M. Gokhale, N. U. Deshpande, D. K. Denzer, J. Liu, Metallurgical Materials Transactions A, 29A (**1998**) 4, 1203

[6] L. F. Mondolfo, Aluminium alloys, Structure and Properties, Butterworts, London 1976

UDK 620.178.1:669.14.018.25
Original scientific article/Izvirni znanstveni članek

ISSN 1580-2949
MTAEC9, 42(5)197(2008)

WEAR MECHANISM OF DUPLEX-COATED P/M VANADIS 6 LEDEBURITIC STEEL

MEHANIZEM OBRABE LEDEBURITNEGA JEKLA P/M VANADIS 6 Z DUPLEKSNO PREVLEKO

Peter Jurči,[1] Mária Hudáková[2]

[1]ECOSOND Ltd.,Prague 5, Czech republic
[2]MtF STU Trnava, Slovak republic
p.jurci@seznam.cz

Prejem rokopisa – received: 2007-11-21; sprejem za objavo – accepted for publication: 2008-02-05

The wear mechanism of duplex-coated P/M Vanadis 6 ledeburitic steel was investigated. Duplex layering by plasma nitriding and PVD CrN coating increased the wear resistance substantially; however, the scattering of the results was too large. The samples differed in the adhesion of the PVD overlay to the nitrided substrate and showed a very different wear resistance and wear mechanism, too. The specimens with good adhesion showed a critical load needed for coating delamination of more than 130 N, low wear, a relatively little damaged PVD layer, and a rapid wear of counterparts. If the adhesion of the coating was smaller, the wear rate increased rapidly and the worn surface showed symptoms of massive cracking and a total collapse of the coating, a strong decrease of the friction coefficient, and of the wear rate of the counterparts.

Key words: ledeburitic P/M steel, duplex coating, wear rate, wear mehanism, coating composition

Raziskan je bil mehanizem obrabe jekla P/M Vanadis 6 z dupleksno prevleko. Dupleksna prevleka iz plazemskega nitriranja in PVD CrNi-prekritja je pomembno povečala odpornost proti obrabi, vendar je bil pri tem prevelik raztros rezultatov. Vzorci so se razlikovali v adheziji med PVD-plastjo in podlago, zato sta bila različna odpornost proti obrabi in mehanizem obrabe. Vzorci z dobro adhezijo so imeli kritično silo za delaminacijo prekritja nad 130 N in relativno majhno obrabo, relativno malo poškodovano PVD-plast in hitro obrabo nasprotnega dela. Pri majhni adheziji prekritja, je hitrost obrabe hitro rastla, obrabljena površina pa je kazala simptome masivnega razpokanja in totalnega kolapsa prekritja, veliko zmanjšanje koeficienta obrabe in hitrosti obrabe nasprotnega dela.

Ključne besede: ledeburitno P/M-jeklo, dupleksno prekritje, hitrost obrabe, mehanizem obrabe, sestava prekritja

1 INTRODUCTION

Ledeburitic steels are widely used in industrial operations like metal cutting, but also in the cold working and sheet-metal forming of large series of parts for the automotive industry. The steels are usually used in the as-heat-treated condition and with a hardness of *HRC* 57–60. Nevertheless, in many cases the heat treatment itself cannot ensure a sufficient service time for the tools and they must be submitted to a surface treatment that also gives them a better resistance to environmental effects.

Thin layers prepared by various PVD (physical vapour deposition) methods are mostly used for the surface treatment of tool steels[1-6]. PVD layers can be deposited over a large range of chemical compositions and mechanical properties, at low temperatures and without any influence on the core properties of the tools. Their common disadvantage is the adhesion to the steel substrate, since PVD layers differ considerably from steels in terms of mechanical and physical properties.

The surface has to meet many criteria to resist various mechanisms of wear. The first of these criteria, and established recently as not the most important, is hardness[1]. The ratio of the hardness to the Young's modulus was established as being the most important criterion for sufficient wear resistance[1]. This ratio differs significantly for steels and for PVD layers, and may cause serious problems in the surface processing of tools. For example, the well-known layers such as TiN, TiAlN and TiB_2 have a hardness of about *HV* 3000 (four times more than tool steels) at a Young's modulus of 400 GPa (2 times higher than steel)[3-5]. Also, for the promising CrN layers, the Young's modulus is higher than that of steels (up to 240 GPa), whereas the hardness can be varied according to the actual chemical composition across a very wide range, from *HV* 1500 to approximately *HV* 2500[6].

The heat treatment affects the Young's modulus in a very limited range. On the other hand, the hardness can be increased very significantly with an appropriate heat treatment. For the steel Vanadis 6, the hardness in the as-delivered state is about *HB* 255 (*HRC* 23)[8], and after heat treatment a hardness of *HRC* 62 (*HV* 750) can be easily achieved. An additional surface hardness increase (and also the hardness/Young's modulus ratio) can be achieved by nitriding. As reported[9,10] for the Vanadis 6 steel after plasma nitriding, a hardness of *HV* 1100 can be achieved. On the other hand, the fracture toughness is lowered very significantly by the nitriding[11,12]. The minimizing of the undesirable effect of nitriding on the fracture toughness is a significant goal of our other

investigations. In this paper we report on the results of an investigation of the wear mechanism of CrN+ plasma-nitriding duplex-layers deposited on a Vanadis 6 substrate.

2 EXPERIMENTAL

Specimens of the steel Vanadis 6 (2.1 % C, 7 % Cr, 6 % V, Fe bal.) were heat treated to a hardness of *HRC* 60, the recommended value for cold-work applications. Plasma nitriding was performed in a RUBIG Micropuls – Plasmatechnik® device at temperatures of 500 °C and 530 °C and processing times of 60 min and 120 min, respectively.

The CrN layers of thickness 2 μm or 5 μm were deposited with vacuum arc sputtering in a Balzers BAI 730M device, and the adhesion of the layers was examined with a scratch test. The microstructural examinations and the analysis of the worn surfaces were performed with scanning electron microscopy. Wear testing was carried out without lubrication using the ring-on-plate configuration of the counterpart and the tested specimen, at loads of 50 N and 150 N, respectively. Hollow cylinders from the ball-bearing steel 100Cr6 heat treated to *HRC* 60 were used as the counterparts. The total movement (sliding in a combination with slow rotation) distance was of 10 km, and the wear weight loss was determined also after (1, 2.5 and 5) km of sliding. Glow discharge optical emission spectroscopy (GDEOS) was used to determine the elements' depth profiles in the near-surface region. The phase constitution of the CrN layers was identified with X-ray diffraction.

3 RESULTS

In a previous paper[13], the best nitriding parameters with respect to the adhesion of the PVD layers were found to be: a temperature of 530 °C, a processing time of 120 min and a reactive atmosphere with the composition $N_2 : H_2 = 1 : 3$. Tribological tests showed a large scatter in terms of the wear resistance. Therefore, it was decided to examine other combinations of nitriding parameters with the aim to reduce the dispersion of results and consider also the possibility of improving of the fracture toughness, although this was the main goal of other investigations.

An example of the microstructure of a duplex-layer (CrN + plasma nitriding) is shown in **Figures 1 and 2**. On the surface, a CrN layer of thickness 5 μm is deposited. The nitrided inter-layer has a thickness of about 40 μm. It differs from the non-nitrided material mainly in the topography caused by the etching. Also, there is a continuous or quasi-continuous layer of nitride found at the boundaries of the original grains. No inhomogeneities were found in the surface regions and the PVD layer was free of cracks and pores.

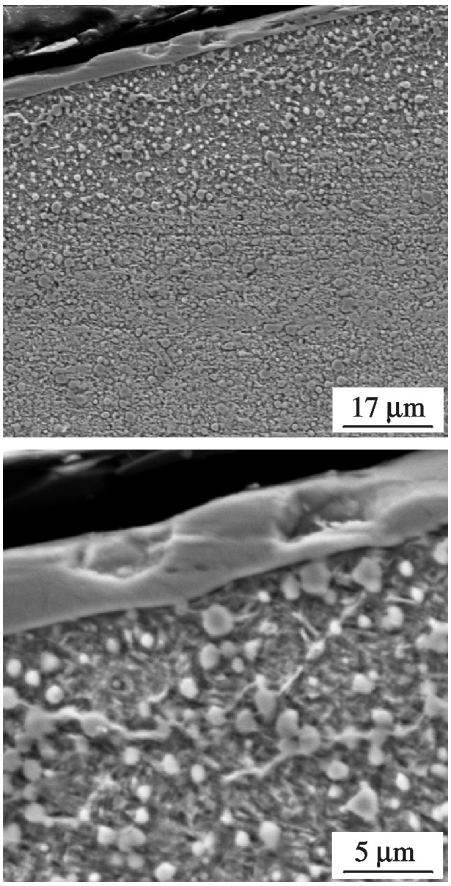

Figures 1, 2: SEM micrographs of duplex layer. Above – overview, below – detail
Slika 1, 2:. SEM-posnetka dupleksnega prekritja. Zgoraj splošni videz, spodaj detajl

As shown in **Table 1**, all the newly used combinations of plasma nitriding and CrN layering produced a minimal adhesion of approximately 50 N. This indicates that the pre-treatment ahead of the plasma nitriding is a promising method for increasing the adhesion of the PVD CrN coating. On the other hand, the adhesion values again exhibited a large dispersion, even for specimens processed under the same conditions.

The results of the measurements of the wear resistance for a load of 50 N in **Figure 3**, demonstrate the good wear behaviour of the duplex-treated material in comparison to a material without surface processing, only nitrided or only CrN layered[9]. When compared to specimens pre-nitrided at 530 °C for 120 min and then CrN layered[14], the results of the tests were not sufficiently reliable. However, it is clear that the pre-nitriding at 500 °C for 120 min. is more efficient for the wear behaviour of the duplex layer than the pre-nitriding at 530 °C for 60 min. Also, in contrast to previous tests,[9,14] it was confirmed that a thinner CrN layer had a better wear resistance. This wear behaviour is to be expected, since internal stresses, often leading to coating damage, increase with the coating thickness under given testing conditions[15].

The measurements gave a lower weight loss for the counterparts after sliding with the CrN layer with a thickness of 2 µm (**Figure 4**). No major changes in weight loss were found, which would indicate that no delamination of the coatings occurred during the sliding test. It is concluded that the cause of the different wear was the differences in the friction coefficient (**Figure 5**). A higher friction coefficient induced rather more wear (**Figure 3**).

Table 1: Measurements of adhesion with a scratch test. Yellow lines – results in[9,14]

Tabela 1: Določanje adhezije s trgalnim preskusom. Rumene vrstice – rezultati v[9,14]

Processing	Lc3/N	Lc4/N	Lc5/N
CrN 2 µm	18	44	60
CrN 5 µm	26	56	65
Nitriding 530 °C/120 min + CrN 2 µm	44	70	not identified
Nitriding 530 °C/120 min + CrN 5 µm	90	94	99
Nitriding 500 °C/120 min + CrN 2 µm	50, not identified	79, 156	116, -
Nitriding 500 °C/120 min + CrN 5 µm	55, 148	not identified	129, 158
Nitriding 530 °C/60 min + CrN 2 µm	46,135	not identified, 100	108, 138
Nitriding 530 °C/60 min + CrN 5 µm	47, 52	not identified	98, 134

The use of a higher load (150 N) led to increasing differences in the wear behaviour between the specimens processed by various combinations of plasma nitriding and CrN layering (**Figure 6**), and also between specimens processed in the same batch (**Figure 8**). However, the general tendency of improved wear resistance after plasma nitriding was retained. The assessment of other

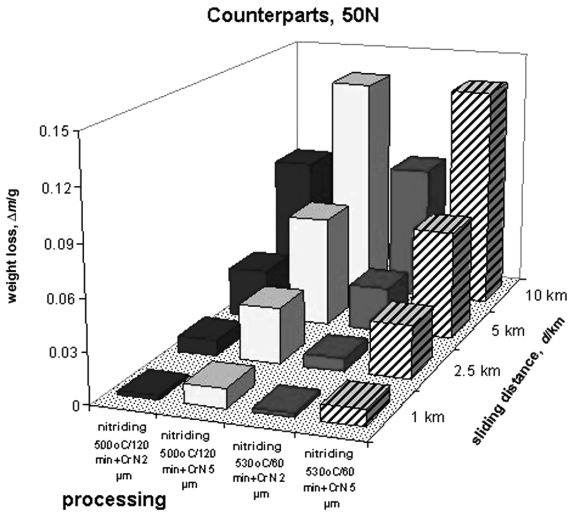

Figure 4: Weight loss of counterparts as a function of sliding distance and surface treatment, load of 50 N

Slika 4: Izguba mase nasprotnega dela v odvisnosti od dolžine drsenja in površinske obdelave; obremenitev 50 N

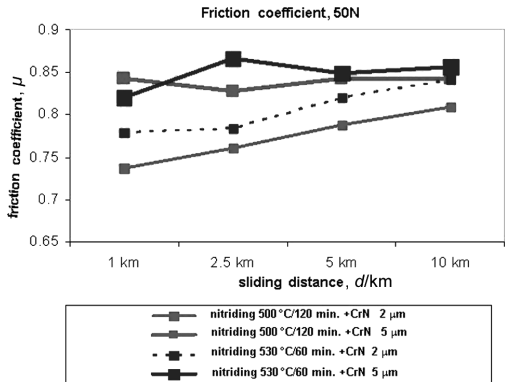

Figure 5: Friction coefficient as a function of sliding distance, load of 50 N

Slika 5: Koeficient trenja v odvisnosti od dolžine drsenja; obremenitev 50 N

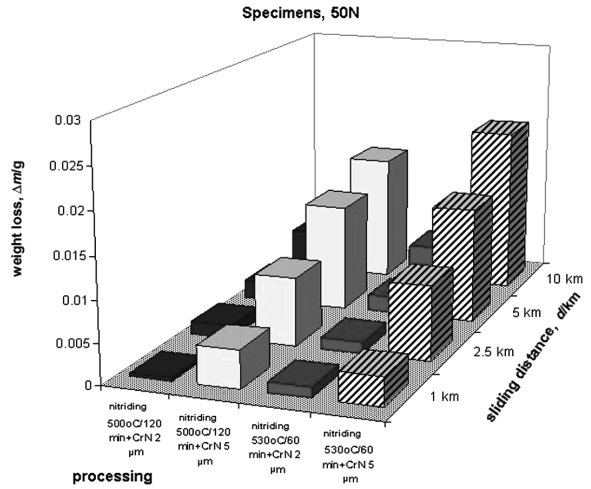

Figure 3: Weight loss of specimens as a function of sliding distance and surface treatment, load of 50 N

Slika 3: Izguba mase vzorcev v odvisnosti od dolžine drsenja in površinske obdelave; obremenitev 50 N

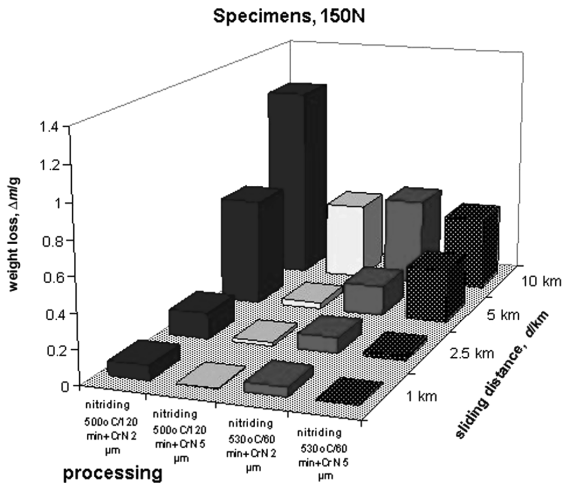

Figure 6: Weight loss of specimens as a function of sliding distance and surface treatment, load of 150 N

Slika 6: Izguba mase vzorcev v odvisnosti od dolžine drsenja in površinske obdelave; obremenitev 150 N

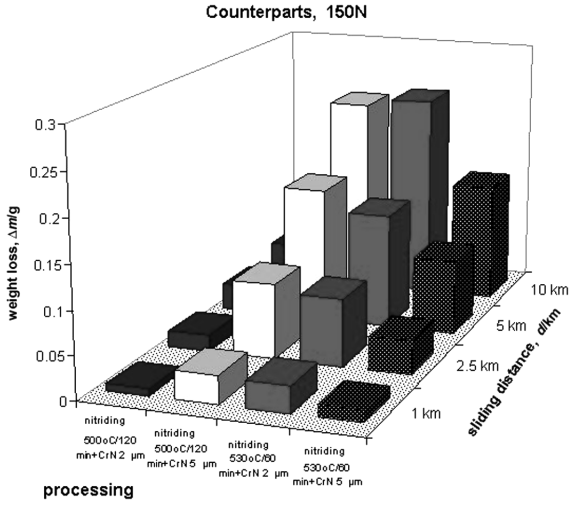

Figure 7: Weight loss of counterparts as a function of sliding distance and surface processing of the specimen, load 150 N

Slika 7: Izguba mase nasprotnega dela v odvisnosti od dolžine drsenja in površinske obdelave vzorca; obremenite 150 N

effects on the wear resistance became more difficult due to sudden changes in the sliding surface due to the PVD-layer delamination. Therefore, the mean values from Figure 6 do not represent the wear behaviour accurately because of the large dispersion due to delamination on at least one specimen from the three tested.

Also, the figures of weight loss for the counterparts exhibited a large scatter. The mean values in **Figure 7** give only partial information about the process during the wear testing. In the cases of an absence of delamination, the weight loss of the specimen was minimal, the counterpart underwent intensive wear (**Figure 8**) and the friction coefficient increased slowly.

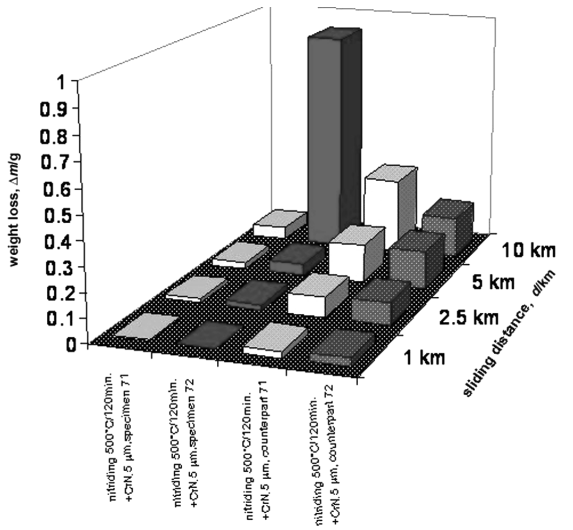

Figure 8: Wear of specimen and counterpart in the case of good (yellow) and poor (red) adhesion

Slika 8: Obraba vzorca in nasprotnega dela za primer dobre (rumeno) in slabe (rdeče) adhezije

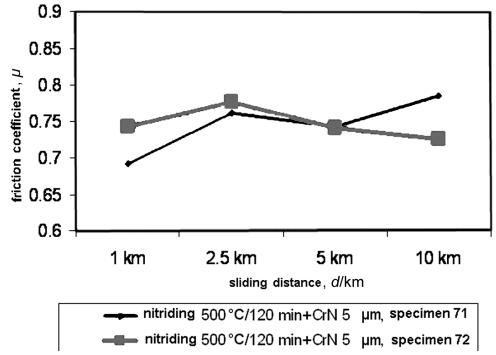

Figure 9: Friction coefficient for the specimen with good adhesion (yellow) and poor adhesion (red) of the CrN coating

Slika 9: Koeficient obrabe za vzorec z dobro (rumeno) in slabo (rdeče) adhezijo CrN-plasti

On the other hand, if the adhesion of the CrN layer was poor, the wear rate on the specimen's side changed suddenly from low to very high, and the weight loss of the counterpart became minimal. Simultaneously, the fiction coefficient also decreased as a result of the decreased surface contact between the specimen and the counterpart (**Figure 9**). To understand these differences in wear behaviour, selected specimens with good (71) and worse (72) adhesion were subjected to a more detailed investigation.

These observations correspond well with the measurements of adhesion from the scratch test, although the type of contact differs for those during the scratch test (point contact of the diamond indenter) and during the wear-resistance test (linear contact of a hollow cylinder with approximately equal hardness) differs considerably. As shown already, the adhesion of 50 N, which is the minimum acceptable value for various industrial applications, was achieved for all the

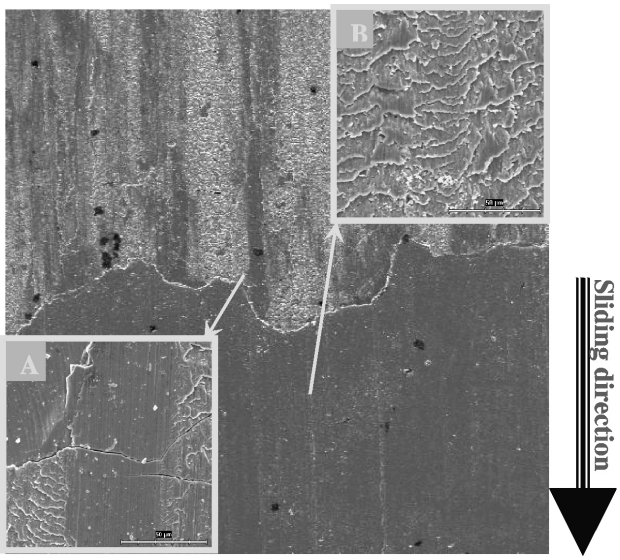

Figure 10: Worn surface of the specimen with good adhesion of the CrN layer

Slika 10: Obrabljena površina vzorca z dobro adhezijo CrN-plasti

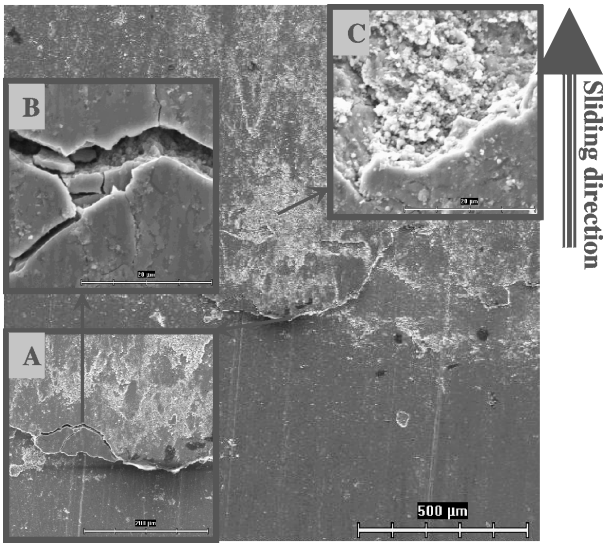

Figure 11: Worn surface with poor adhesion of the CrN layer
Slika 11: Obrabljena površina vzorca s slabo adhezijo CrN-plasti

specimens. Large differences in the wear resistance found for a load of 150 N can be attributed to the scattering of the adhesion values (ranged from 50 N to 148 N) determined during the scratch test.

Figure 10 shows the surface of a specimen with excellent PVD layer adhesion. The surface shows two areas of different micro-morphology. The first area (part A) is typical for the practically undamaged layer and only the friction producing parallel tracks in the sliding direction occurred during the wear test. On the second, "B", area a slightly deformed and cracked coating without clear marks of delamination is found. The preservation of the coating on the surface in spite of the high contact pressure confirms its excellent adhesion.

In the case of worse adhesion of the coating, the situation is significantly different (**Figure 11**). The wear process was probably equal to the case of good adhesion (**Figure 10**) until the occurrence of cracking in the CrN layer at various places. This was mostly, however, at the boundary between the worn and the unaffected parts of the specimen (A). From this moment on the friction coefficient started to decrease (**Figure 9**). The degradation of the layer continued with its crumbling, predominantly in the vicinity of the primary cracks (B), up to the total material removal in selected areas (C). The removed fragments of the CrN coating accelerated the weight loss on the specimen's side due to the removal itself, while on the counterpart's side, the weight loss was practically stopped due to minimizing of the sliding contact (minimizing of the surface undergoing the wear) and lowering of the friction coefficient (**Figure 9**).

Specimens with good (71) and poor (72) wear behaviour also differ in the chemistry of the PVD layers and, as a consequence, in the phase constitution, too. The CrN layer on specimen 71 contains less chromium than that on specimen 72 (**Figures 12 and 13**), but it has more nitrogen. The difference is 1.5–2.0 %, depending on the depth. At the same time, the layer on specimen 71 consists mainly of the Cr_2N compound, while in the layer on specimen 72, the content of nitrogen in the chromium solid solution is significantly increased (**Figure 14**). The specimens also differ in terms of the texture of the layer. The diffraction peaks of $Cr_2N_{(110)}$ at 37° of the two-theta angle and $Cr_2N_{(300)}$ at 67° are higher for specimen 72, with a poor adhesion, than for specimen 71, with good adhesion. The differences indicate a different mechanism of growth for both layers. At first sight this is surprising, since the layers were prepared on specimens processed in the same way as in the heat-treatment stage and in the nitriding stage.

Another possible explanation of the different wear behaviour of the specimens, and also of those processed under the same processing conditions, is a possible exceeding of the load-carrying capacity of the substrate. Nevertheless, the scratch test indicated a large scatter of the critical load values and, therefore, the differences in the layer formation displayed by X-ray diffraction

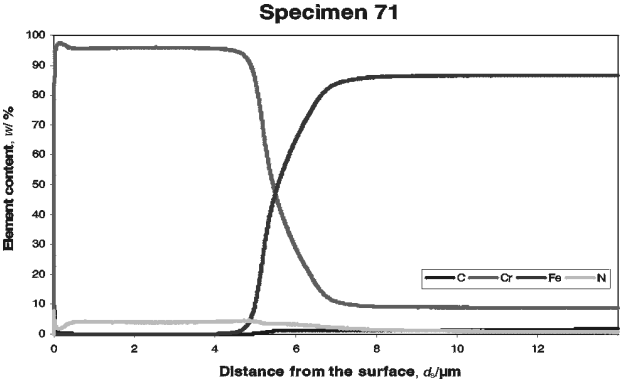

Figure 12: Depth profiles of elements throughout the near-surface region – specimen with good adhesion
Slika 12: Porazdelitev elementov v CrN-plasti blizu površine, vzorec z dobro adhezijo

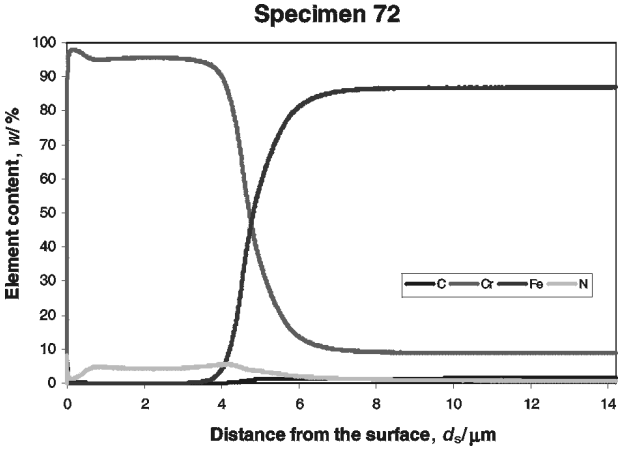

Figure 13: Depth profiles of elements throughout the near surface region – specimen with poor adhesion
Slika 13: Porazdelitev elementov v CrN-plasti blizu površine, vzorec s slabšo adhezijo

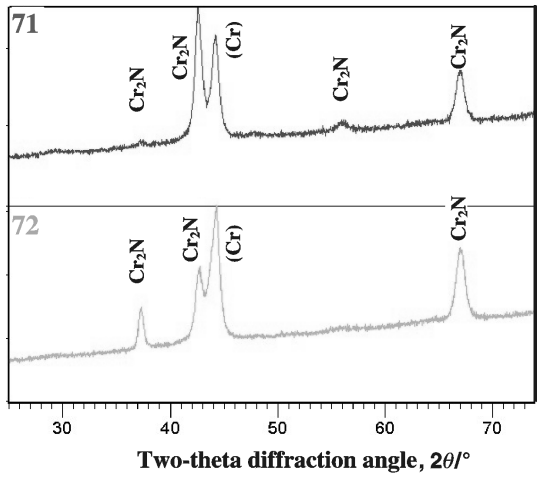

Figure 14: X-ray diffraction patterns from PVD CrN layers
Slika 14: Difraktogram rentgenskih žarkov v PVD-plasti

measurements are more probably the primary explanation for the different wear resistance of the specimens. The cause of different layer growth, in a given batch, too, can probably be attributed to the positional effect of the specimen with respect to the chromium source (target) during the sputtering. No other effects with a possible influence on the layer growth are known.

4 CONCLUSIONS

1) For all the combinations of plasma nitriding and CrN coating, the critical load measured with the scratch test was at least 50 N, which is considered to be an acceptable value for industrial applications. In some cases the adhesion was much better and the critical load exceeded 130 N. However, a large scatter of adhesion values was found, also for specimens processed under the same nitriding and/or coating conditions.

2) Wear testing at a load of 50 N did not show a significant scatter of results. The wear of specimens proceeded in a steady manner and slightly better results were found for the thinner CrN layers.

3) The use of a load of 150 N emphasized the difference in the wear behaviour of the specimens, also for those prepared under the same processing conditions. For the specimens with excellent adhesion, the wear rate on the specimen's side was low and on the counterpart's side it was much greater. The friction coefficient increased slightly with the increased sliding distance. For the specimens with poor adhesion, a sudden and dramatic increase in the wear rate on the specimen's side occurred during the test. This increase is connected with the decrease of the friction coefficient and the lowering of the wear on the counterpart's side.

4) In the case of specimens with excellent adhesion the CrN coating remained on the surface, although in a slightly damaged form. Coatings with small adherence cracked and were progressively removed from the contact surface.

5) Layers with excellent adhesion differ from those with poor adhesion in chemistry and phase constitution. In the first there was less chromium in the solid solution and more Cr_2N compound was found in the second. Moreover, the different texture probably also indicates a difference in the growth mechanism.

ACKNOWLEDGEMENTS

Authors wish to thank the Ministry of Education and Youth of the Czech Republic and the Slovak Republic for the financial support for the solution of the Project Eureka E!3437 PROSURFMET.

5 REFERENCES

[1] Oberle, T.: J. of Metals, (**1951**) 3, 438–439
[2] Matthews, A., Leyland, A.: *HTM* 56 (**2001**) 1, 5
[3] Kříž, A., Zetek, M.: In.: Proc. of the Conf. Vrstvy a povlaky 2004, Rožnov pod Radhoštěm, 7.–8. 10. 2004, 12
[4] Šmíd, M. et al.: In: Proc. of the Conf. Vrstvy a povlaky 2004, Rožnov pod Radhoštěm, 7.–8. 10. 2004, 79
[5] Podgornik, B. et al.: Wear 254 (**2003**), 1113
[6] Sokovič, M., Panjan, P., Kirn, R.: J. Mater. Proc. Techn., 157–158 (**2004**), 616
[7] Salas, O. et al.: Surf. Coat. Techn. 172 (**2003**), 117
[8] Vanadis 6 – SuperClean, Uddeholm Tooling AB, Sweden, 2001
[9] Jurči, P., Panjan, P.: Surface Processing of the PM Vanadis 6 Steel with Plasma Nitriding and CrN PVD – Coating, In: Proceedings of the *European Powder Metallurgy Congress*, Prague, Czech Republic, 2005
[10] Jurči, P., Hnilica, F., Suchánek, J., Stolař, P.: Structural Features of the Cr-V Ledeburitic Steel Saturated by Nitrogen, *Mater. Tehnol.,* 38 (**2004**) 1–2, 13
[11] Hnilica, P., Čmakal, J., Jurči, P.: Alterations in Fracture Behaviour of the Cr-V Ledeburitic Steel Vanadis 6 Caused by Plasma Nitriding, In.: *11th Conference on Materials and Technology,* book of abstracts, Portorož, Slovenia, October 1–3, 2003
[12] Jurči, P., Hnilica, F., Čmakal, J., Pechmanová, J.: In: Proceedings of the 8th National Conference *Degradation of Structural Materials,* September 2.-4, 2003, Terchová, Slovakia, p. 137
[13] Jurči, P., Musilová, A., Stolař, P., Hrubý, V.: In: Proceedings of the Conference *Carburizing and Nitriding*, November 27–28, 2001, Brno, Czech Republic, p. 81
[14] Jurči, P., Hudáková, M.: Surface Processing of the PM Vanadis 6 Steel with Plasma Nitriding and CrN PVD – Coating, In: Proceedings of the 16th Int. Conf. Metal 2007, May 2007, Hradec n. Moravicí, Czech Republic, CD – ROM
[15] Diao, D. F. et al.: The Maximum Tensile Stress on a Hard Coating Under Sliding Friction. Tribology Intern., 27 (**1994**) 4, 267–272

UDK 669.14.018.252:669.715:539.42
Izvirni znanstveni članek/Original scientific article

ISSN 1580-2949
MTAEC9, 42(5)203(2008)

ANALIZA TOPLOTNIH RAZPOK NA ORODJIH ZA TLAČNO LITJE ALUMINIJA

ANALYSIS OF THERMAL CRACKS ON DIE CASTING DIES

Damjan Klobčar[1], Janez Tušek[1], Matej Pleterski[1], Ladislav Kosec[2], Mitja Muhič[3]

[1]Fakulteta za strojništvo, Univerza v Ljubljani, Aškerčeva 6, 1000 Ljubljana, Slovenija
[2]Naravoslovnotehniška fakulteta, Univerza v Ljubljani, Aškerčeva 12, 1000 Ljubljana, Slovenija
[3]TKC d.o.o., Trnovska 8, 1000 Ljubljana, Slovenija

Prejem rokopisa – received: 2007-09-21; sprejem za objavo – accepted for publication: 2008-02-05

Podaljšanje trajnostne dobe orodij je ekonomsko zelo pomembno, zato smo raziskali poškodbe orodij za tlačno litje aluminijevih zlitin. Analizirali smo vzroke in mehanizme nastanka razpok, ki nastanejo zaradi temperaturnega utrujanja med tlačnim litjem. Izdelali smo napravo za potopni preskus, ki omogoča simulacijo pogojev med tlačnim litjem teh zlitin in kontrolirano temperaturno utrujanje jekla. Epruvete iz jekla H13 so bile različno toplotno obdelane. Na vogale nekaj epruvet je bilo po postopku TIG navarjeno jeklo maraging, ki je bilo preskušano v navarjenem stanju in optimalno staranem stanju. Po določenem številu ciklov so bile površine epruvet vizualno pregledane, vzorci pa so bili razrezani in pregledani na svetlobnem in vrstičnem elektronskem mikroskopu. Področja okoli razpoke so bila analizirana z energijsko disperzijsko spektroskopijo rentgenskih žarkov (EDS). V vogalu epruvete smo izmerili število in velikost razpok ter padec trdote. Rezultati so pokazali, da je odpornost jekla proti temperaturnemu utrujanju odvisna od vrste jekla in njegove toplotne obdelave. Dobro odpornost proti temperaturnemu utrujanju ima kakovostno toplotno obdelano jeklo H13. Širjenje površinskih razpok dodatno pospeši oksidacija površine.

Ključne besede: tlačno litje, aluminijeve zlitine, termično utrujanje, potopni preskus, orodno jeklo za delo v vročem, jeklo maraging

The aim of this research was to analyse the aluminum alloy die casting die failures with the aim of prolonging in-service die life. An extensive analysis of thermal fatigue cracks in aluminium alloy die casting was performed. An immersion test apparatus was developed that enables the simulation of conditions during aluminum alloy die casting and the controlled thermal fatigue testing of materials. Specimens of the AISI H13 tool steel were differently heat treated. On the edges of some specimens, the maraging steel was gas tungsten arc (GTA) weld cladded. These samples were tested in as-welded and in optimally aged condition. After completion of a particular number of cycles, the specimen edge surface was examined visually. The specimens were then cut and examined with light and scanning electron microscopy (SEM). The energy-dispersive X-ray spectroscopy (EDS) mapping of areas around the cracks was performed, also, and the number and length of thermal fatigue cracks were assessed and Vickers hardness profiles were determined. The results confirmed the good thermal fatigue resistance of the properly hardened H13 steel. The surface cracks growth is accelerated by surface oxidation.

Keywords: aluminium alloy, die casting, thermal fatigue cracking, immersion test, hot work tool steel, maraging steel

1 UVOD

Tlačno litje aluminijevih zlitin je velikoserijski postopek izdelave izdelkov zahtevnih geometrijskih oblik v ozkih dimenzijskih tolerancah. Med tlačnim litjem priteče v orodje talina s hitrostjo od 30 m/s do 100 m/s in s temperaturo okoli 700 °C. Polnilni tlaki so od 50 MPa do 80 MPa [1]. Trajnost orodij zmanjšujejo a) temperaturni cikli, ki povzročajo temperaturne razpoke na površini orodja zaradi temperaturnega utrujanja jekla, b) korozija in sprijemanje zaradi oksidacije aluminija na površino gravure [2,3,] c) erozija zaradi toka taline, č) prelomi orodja zaradi temperaturnih šokov in d) segrevanje jekla, ki povzroča nestabilnost mikrostrukture in degradacijo mehanskih lastnosti [4-7].

Orodja za tlačno litje aluminija se najpogosteje poškodujejo zaradi razpok, ki nastanejo zaradi temperaturnega utrujanja jekla. Razpoke, ki se pojavijo v orodju, povzročajo nesprejemljive odtise na površini izdelka.

Trajnost orodja lahko podaljšamo a) z zmanjšanjem temperaturnih napetosti med obratovanjem orodja, b) izbiro jekla in toplotno obdelavo, ki zagotavljata večjo odpornost proti temperaturnemu utrujanju, c) s površinskimi prevlekami na orodjih in č) reparaturnim varjenjem, s katerim saniramo poškodovano orodje. Delovne napetosti v orodju zmanjšamo z bolj blagimi parametri tlačnega litja, optimalnim notranjim segrevanjem orodja (temperiranjem), z optimalno geometrijo izdelka/orodja s čim manj ostrimi prehodi ter z minimalnim vnosom zaostalih napetosti med njegovo izdelavo. Površinske prevleke uspešno zmanjšujejo korozijo, spajanje in erozijo površine gravure, vendar niso odporne proti temperaturnemu utrujanju [8]. Novo razvite večslojne prevleke že dosegajo izboljšano odpornost proti temperaturnemu utrujanju [9,10].

Poleg klasičnih CrMoV-jekel za delo v vročem, imajo dobro vzdržljivost tudi orodja, izdelana iz jekel maraging z nižjo vsebnostjo niklja (od 10 % do 14 %) [11,12]. Njihova prednost pred klasičnimi orodnimi jekli za delo v vročem sta manjši modul elastičnosti in manjši temperaturni raztezek, kar oboje zmanjšuje temperaturne napetosti. Večja toplotna prevodnost jekel maraging poveča prevajanje toplote po materialu in s tem zmanjšuje

temperaturne gradiente in napetosti, kar lahko prispeva k daljši obratovalni dobi orodja.

Razvoj orodnih jekel za delo v vročem gre v smeri izboljšanja stabilnosti mehanskih lastnosti v obratovanih razmerah [12]. K temu veliko prispevajo toplotne obdelave, ki preprečujejo oz. zavirajo spremembe mikrostrukture z oblikovanjem bolj stabilnih karbidnih izločkov (M(CrMoV)C) med popuščanjem. Naloga teh izločkov je zaviranje gibanja dislokacij, kar povečuje odpornost jekla proti mehčanju [13-15].

Raziskave na področju napovedovanja trajnosti orodij [13,14,16,17] in opisa mehanizmov poškodb [5,18,19] potekajo v realnih razmerah na orodjih med obratovanjem ali v laboratorijskih razmerah. Ugotavljanje odpornosti jekla proti temperaturnemu utrujanju izvajamo s preizkusi izotermnega utrujanja (pri konstantni temperaturi se spreminja obremenitev), termomehanskega utrujanja in temperaturnega utrujanja v najrazličnejših izvedbah [14,20-22].

2 EXPERIMENTALNI DEL

Preizkušali smo jeklo 1.2344 (kemične sestave: 0,4 % C; 5,15 % Cr; 1,05 % Si; 0,4 % Mn; 1,35 % Mo in 1 % V) ter vare iz jekla maraging 1.6356 (kemične sestave: 0,02 % C; 1,35 % Mo; 18 % Ni; 12 % Co; 0,1 % Al in 1,6 % Ti).

2.1 Potopni preizkus

Naredili smo napravo za potopni preizkus (PP) temperaturnega utrujanja, ki omogoča kontrolirano temperaturno utrujanje jekla (**slika 1a**). Cikel je trajal 21 s in je zajemal trisekundno držanje epruvet v emulziji (32 °C), ki prepreči sprijemanje aluminija na epruvete, štirisekundno gibanje epruvet do posode z raztaljeno aluminijevo zlitino, desetsekundno držanje epruvet v tej zlitini s temperaturo ≈ 700 °C in štirisekundno vračanje epruvet do posode z emulzijo. Epruvete so bile vseskozi notranje hlajene z vodo s temperaturo 20 °C. To povzroča velike tlačne napetosti na površini epruvete, ko je le-ta potopljena v talino aluminijeve zlitine, in natezne napetosti, ko je epruveta potopljena v hladno emulzijo. Največje napetosti se pojavijo v vogalu epruvete.

Velike tlačne napetosti povzročijo v vogalu epruvete plastično deformacijo, saj napetosti krepko presegajo tiste pri tečenju jekla pri tej temperaturi [24]. V hladni fazi cikla, ko je epruveta pomočena v hladno emulzijo, nastanejo natezne napetosti, ki povzročajo nukleacijo razpok. Razpoke nato rastejo zaradi malocikličnega utrujanja.

2.2 Oblika in priprava epruvet

Preizkusili smo dve obliki epruvet: klasično za potopni preskus (**slika 1b**) in epruveto z optimalno oblikovanim vogalom (**slika 1c**). Slednjo smo razvili na osnovi analize napetosti z metodo končnih elementov (MKE) in omogoča večje temperaturne gradiente oz. napetosti med potopnim preskusom ter bolj zahtevne pogoje preskušanja. Z navojem M16 je bila epruveta pritrjena na pnevmatski manipulator.

Epruvete so bile izdelane iz jekla H13 in toplotno obdelane, tj. kaljene in popuščene (**tabela 1**). Toplotna obdelava 1 pomeni kakovostno toplotno obdelavo s kaljenjem v vakuumu, toplotna obdelava 2 pa toplotno obdelavo slabše kakovosti, s kaljenjem na zraku. Na nekaj epruvet, kaljenih v vakuumu, smo po postopku TIG navarili jeklo maraging. Varjenje je potekalo v zaščitni atmosferi plina argona s pretokom 10 L/min. Varilni tok je bil 82 A, varilna napetost 11 V, čas varjenja je bil okoli 150 s, vnos energije pa okoli 1185 J/mm. Nekaj epruvet smo po varjenju starali 3 h pri temperaturi 480 °C, druge pa so bile preskušene v navarjenem stanju. Epruvete so bile mehansko obdelane (**slika 1c**).

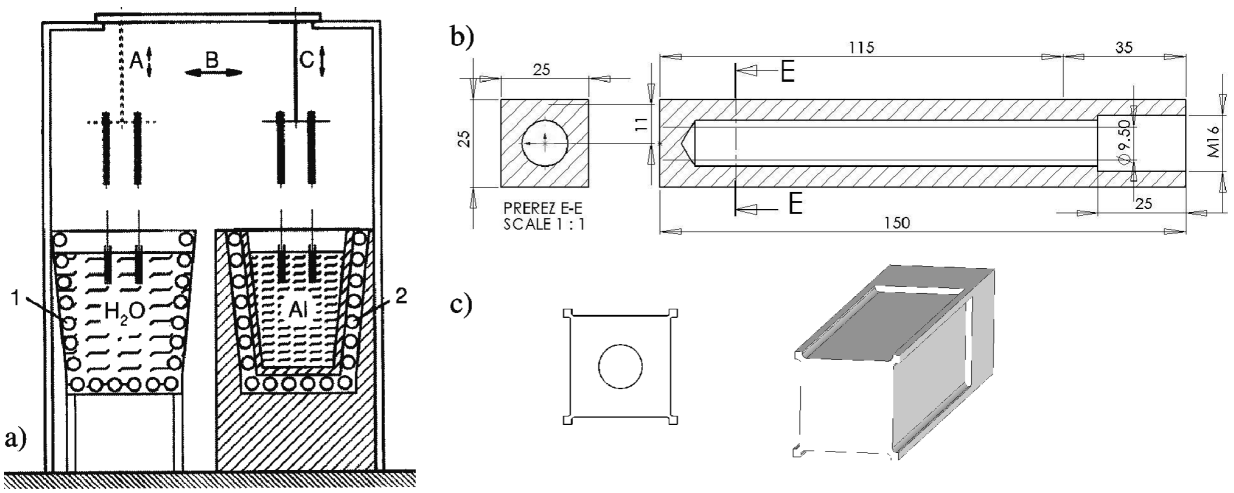

Slika 1: a) Shematski prikaz naprave za termično utrujanje materiala, b) klasična epruveta za preskušanje in c) optimalna oblika epruvete
Figure 1: a) Scheme of the thermal fatigue test apparatus, b) shape of the classic thermal fatigue test specimen, and c) optimal test specimen geometry

2.3 Preskušanje in vrednotenje podatkov

Z epruvetami smo naredili 20 000 preizkusov temperaturnega utrujanja. Robove epruvet smo po vsakih 4 000 ciklih vizualno pregledali, ali so razpokani. Po 20 000 ciklih smo epruvete razrezali preko vogala vzdolž njene dolžine (**slika 4 a**) in naredili mikroobruse. Vzorce smo jedkali v 4-odstotni raztopini nitala. Analizirali smo mikrostrukturo, izmerili profil mikrotrdote po Vickersu od vogala epruvete proti centru ter na svetlobnem mikroskopu fotografirali in v programu Image Tool analizirali dolžino in število razpok vzdolž prerezanega vogala epruvete. Izmerjene vrednosti smo statistično obdelali. V vrstičnem elektronskem mikroskopu (SEM) Jeol-JSM 5610 smo z elektronsko mikroanalizo izmerili kemično sestavo materiala na površini in v okolici razpoke.

2.4 Analiza z metodo končnih elementov

Z MKE in s programom ABAQUS smo simulirali temperaturno utrujanje [23]. Naredili smo sekvenčno vezano termomehansko analizo in določili optimalno obliko epruvete ter zahtevne pogoje potopnega preizkusa [22].

3 REZULTATI

3.1 FEM-analiza

Toplotne napetosti (**slika 2 b**) med potopnim preskusom so posledica temperaturnih gradientov (**slika 2 a**) med površino in notranjostjo epruvete. Največji gradienti temperature oz. napetosti se pojavijo na površini v začetku pomakanja epruvete v vročo talino in hladno emulzijo. Kasneje se le-ti zmanjšajo zaradi prenosa toplote v notranjost epruvete. Posledice cikličnega obremenjevanja epruvet so bile vidne kot razpoke na površini.

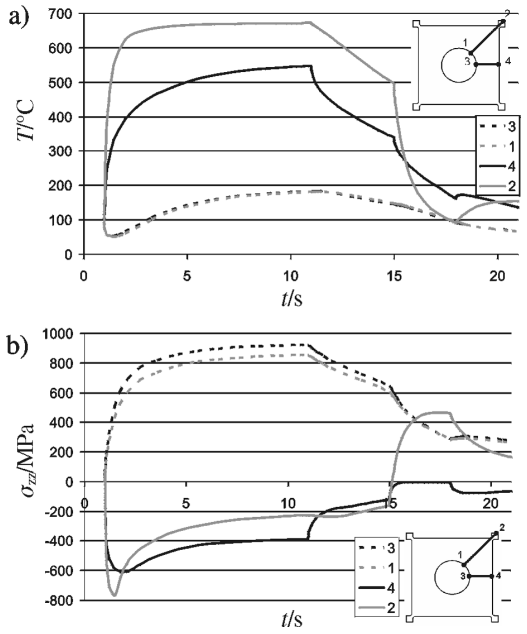

Slika 2: MKE-analiza a) temperatur in b) napetosti v epruveti med potopnim preskusom. Parametri potopnega preskusa: T_{AL} = 690 °C, t_{AL} = 10 s, T_{ZRAK} = 28 °C, t_{ZRAK} = 4 s, $T_{EMULZIJA}$ = 32 °C, $t_{EMULZIJA}$ = 3 s, $T_{HLADILNA\ VODA}$ = 20 °C, t_{CIKLA} = 21 s

Figure 2: Finite element analysis of a) temperatures and b) stresses in test specimen during the immersion test. Immersion test parameters: T_{AL} = 690 °C, t_{AL} = 10 s, T_{AIR} = 28 °C, t_{AIR} = 4 s, $T_{EMULSION}$ = 32 °C, $t_{EMULSION}$ = 3 s, $T_{COOLING\ WATER}$ = 20 °C, t_{CYCLE} = 21 s

3.2 Površinske razpoke

Majhno število dolgih razpok se je pojavilo v jeklu H13, kaljenem na zraku (**slika 3 a**). V enakem jeklu, kaljenem v vakuumu, se je pojavilo večje število krajših razpok (**slika 3 b**). V jeklu maraging v navarjenem stanju (**slika 3 c**) in staranem stanju (**slika 3 d**) se je pojavilo veliko število kratkih in komaj opaznih razpok.

3.3 Razpoke v prerezu vogala

Razpoke v epruveti iz jekla H13, kaljeni na zraku, so bile velike in redke (**slika 4 b in 3 a**). Njihova velikost je bila posledica razogljičenja površine pri segrevanju pred kaljenjem in ima manjšo trdoto (**slika 5**) in slabše mehanske lastnosti. Čela (vrhovi) razpok so bila najbolj pogosta na prehodu delno razogljičenega v naogljičeno jeklo (**slika 4 b**). V vogalu epruvete iz jekla H13, ki je bila toplotno obdelana v vakuumu, so bile razpoke bistveno krajše (**slika 4 c**). Podobno velja tudi za površinske navare jekla maraging v navarjenem (**slika 4 d**) in staranem stanju (**slika 4 e**).

3.4 Trdota jekla na površini epruvete

Razen pri epruveti iz jekla H13, ki je bila kaljena v vakuumu, se je pomemben padec trdote pojavil pri vseh

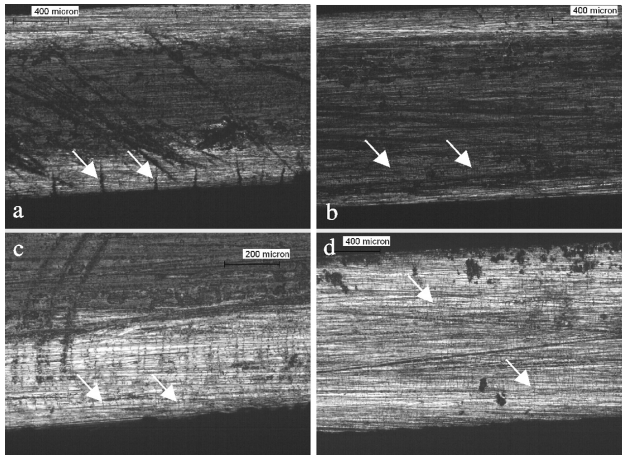

Slika 3: Mikrorazpoke na površini vogala epruvet po 20 000 ciklih: a) jeklo H13, kaljeno na zraku, b) jeklo H13, TO v vakuumu, c) jeklo maraging v navarjenem stanju in d) navarjeno jeklo maraging starano 3 h na temperaturi 480 °C

Figure 3: Micro-cracks on the edge surface after 20 000 cycles of immersion: H13 tool steel quenched in a) air and b) vacuum and maraging steel in c) as-welded condition and d) welded and aged 3 h at 480 °C

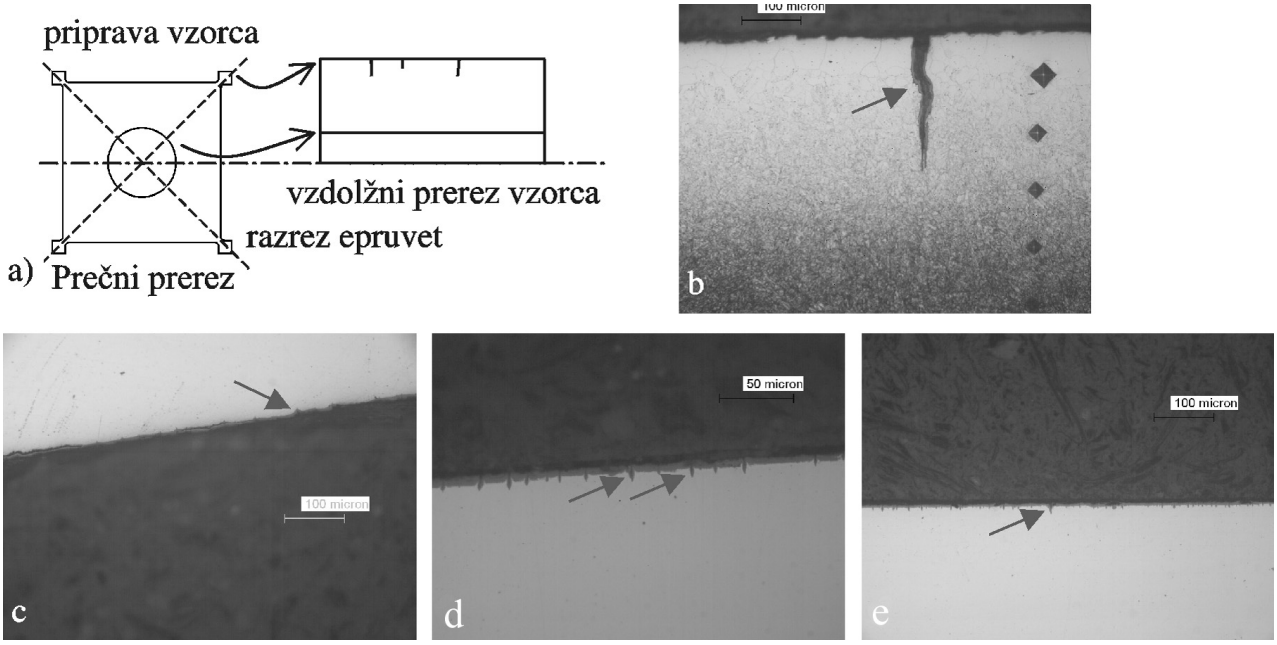

Slika 4: Razpoke na vzdolžnem prerezu kvadrastega vzorca za preizkušanje temperaturne utrujenosti: a) priprava vzorca, b) jeklo H13, kaljeno na zraku, c) H13, TO v vakuumu, d) jeklo maraging v navarjenem stanju in e) navarjeno jeklo maraging starano 3 h na temperaturi 480 °C

Figure 4: Edge cracks at along immersion test specimen. a) Sample preparation, b) H13 tool steel air quenched, c) H13 tool steel vacuum quenched, d) as-welded maraging steel, and e) maraging steel welded and aged for 3 h at 480 °C

analiziranih epruvetah (**slika 5**). Največje zmanjšanje trdote ($\Delta HV \approx 280$) smo opazili v jeklu H13, kaljenem na zraku (**slika 4 b**). Nekoliko manjša padca trdote sta se pojavila v navarih iz jekla maraging ($\Delta HV \approx 180$) kot posledica prestaranja.

3.5 Število in velikost razpok

Najdaljše razpoke so bile v jeklu H13, kaljenem na zraku (**slika 6**). Njihova povprečna dolžina je bila 72,8 µm, najdaljše pa so bile dolge 230 µm (**slika 6 a**). Povprečna gostota razpok v vogalu je bila okoli 4,7 razpoke na milimeter dolžine vogala. Razpoke v drugih epruvetah so bile bistveno krajše. Pri jeklu H13, ki je bilo kaljeno v vakuumu, je bila povprečna dolžina 2,3 µm, pri jeklu maraging v navarjenem stanju 3,7 µm ter pri staranem jeklu maraging 5,2 µm. Povprečna gostota

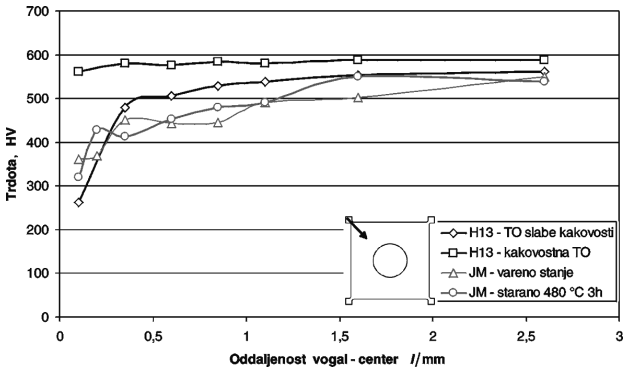

Slika 5: Potek trdote od površine vogala proti centru epruvete po preizkusu utrujanja

Figure 5: Hardness profile from the edge to the centre of the specimen after the immersion test

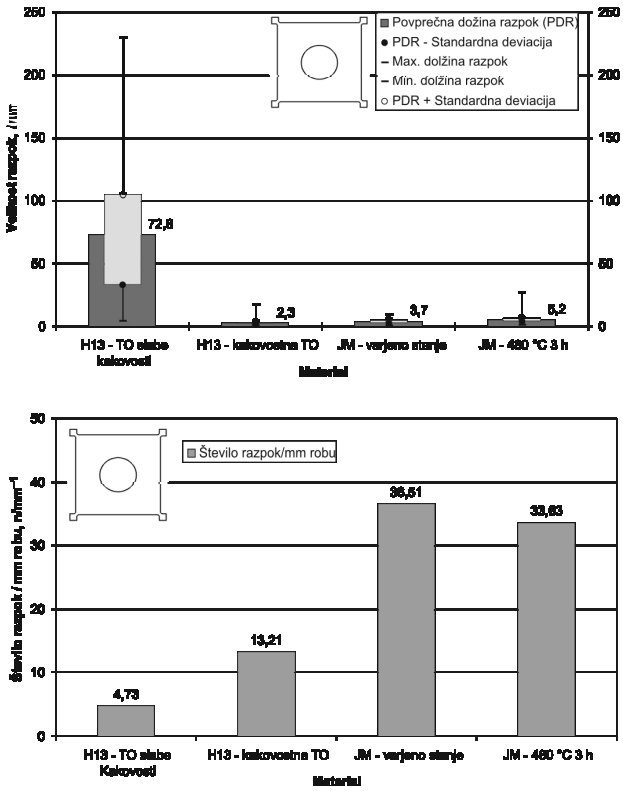

Slika 6: Velikost razpok a) in število razpok b) na dolžini milimetra robu

Figure 6: Edge crack a) length and b) density

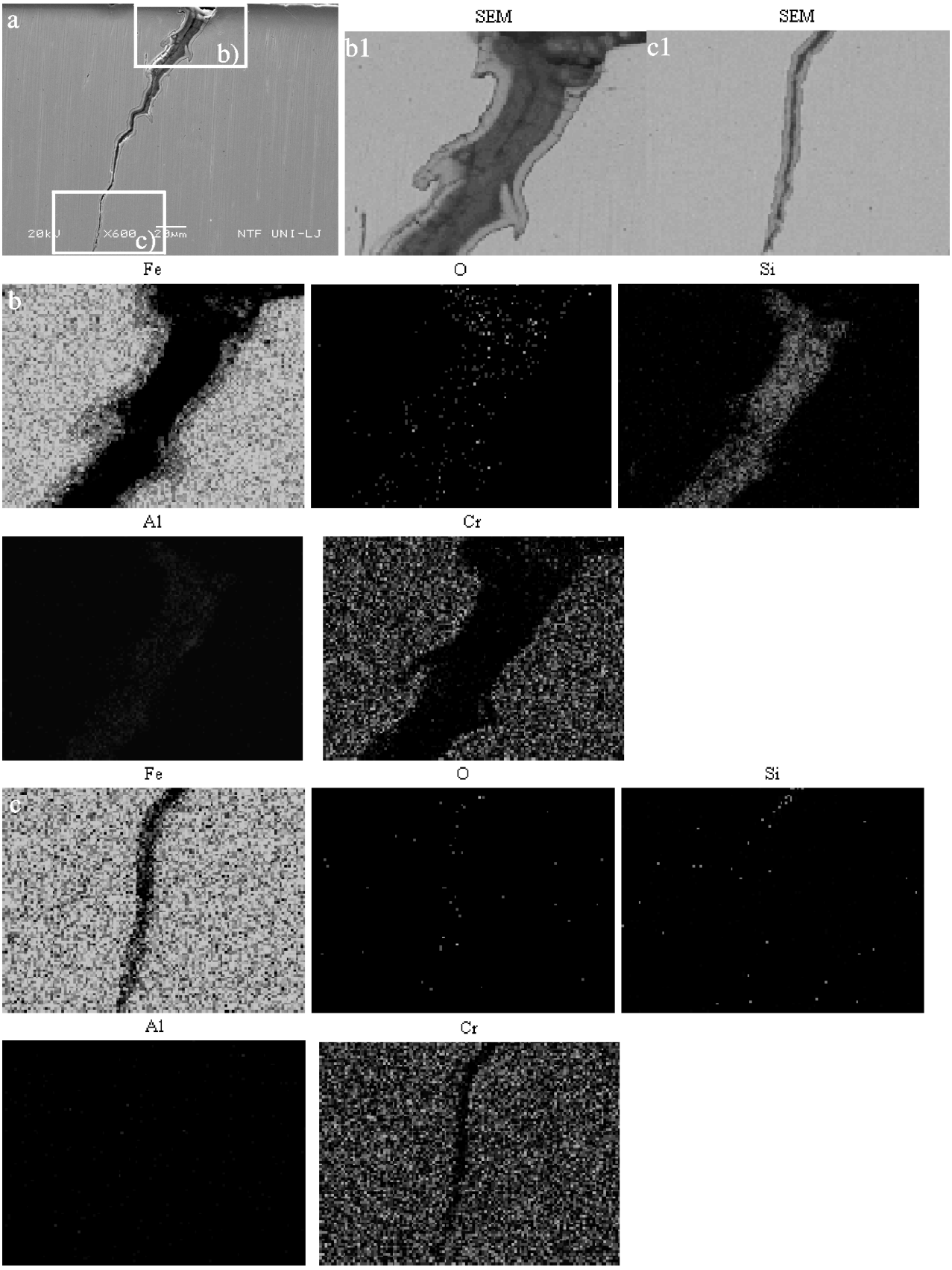

Slika 7: Kemična sestava jekla v okolici oksidnega klina, EDS (jeklo H13)
Figure 7: Chemical composition of steel in the area of the oxide wedge, EDS (H13 tool steel)

razpok na dolžino robu je bila pri jeklu H13, ki je bilo kaljeno v vakuumu, 13,2 mm^{-1}, pri jeklu maraging v navarjenem stanju 36,5 mm^{-1}, pri jeklu maraging v staranem stanju pa 33,6 mm^{-1}.

3.6 Kemična mikroanaliza jekla v okolici razpok

Z energijsko disperzijskim spektrometrom rentgenskih žarkov smo analizirali kemično sestavo materiala v okolici razpok. Značilna kemična sestava jekla H13 ob razpoki po 20 000 ciklih PP je prikazana na sliki 7. Na temenu razpoke (**slika 7 b**) je povečana koncentracija Al in Si, kar kaže, da je teme razpoke zapolnjeno z aluminijevo zlitino, analiza pa je pokazala tudi sledi ogljika in kisika. V oksidni plasti ob razpoki je povečana koncentracija kroma. Podobno je tudi v konici razpok (**slika 7 c**). Kisik penetrira po razpoki do same konice in povzroča oksidacijo. V konici razpoke nismo zaznali sledi aluminija iz taline zaradi ozke razpoke in večje oddaljenosti od vrha.

Kemična sestava okolice razpoke iz jekla maraging, staranega 3 h pri temperaturi 480 °C ter po 20 000 ciklih PP je prikazana na **sliki 8**. Razpoka je imela na površini plast oksidov železa, ki je nastala zaradi difuzije železa iz podpovršinske plasti h kisiku. Podpovršinka plast je bila obogatena z nikljem in kobaltom, ki difundirata v jeklo iz oksidirane plasti železa. V kratkih razpokah so bile sledi silicija in aluminija.

4 DISKUSIJA

4.1 Toplotne razpoke

Nastajanje temperaturnih razpok lahko razdelimo v tri korake; (1) nukleacija, (2) rast razpok in (3) porajajoča rast razpok do porušitve oz. luščenja površine [5]. Tvorba razpok je tesno povezana z lokalno plastično deformacijo na površini jekla, kar je značilno za malociklično utrujanje. Rast razpok pospeši oksidacija razpokane površine z večanjem volumna te plasti,

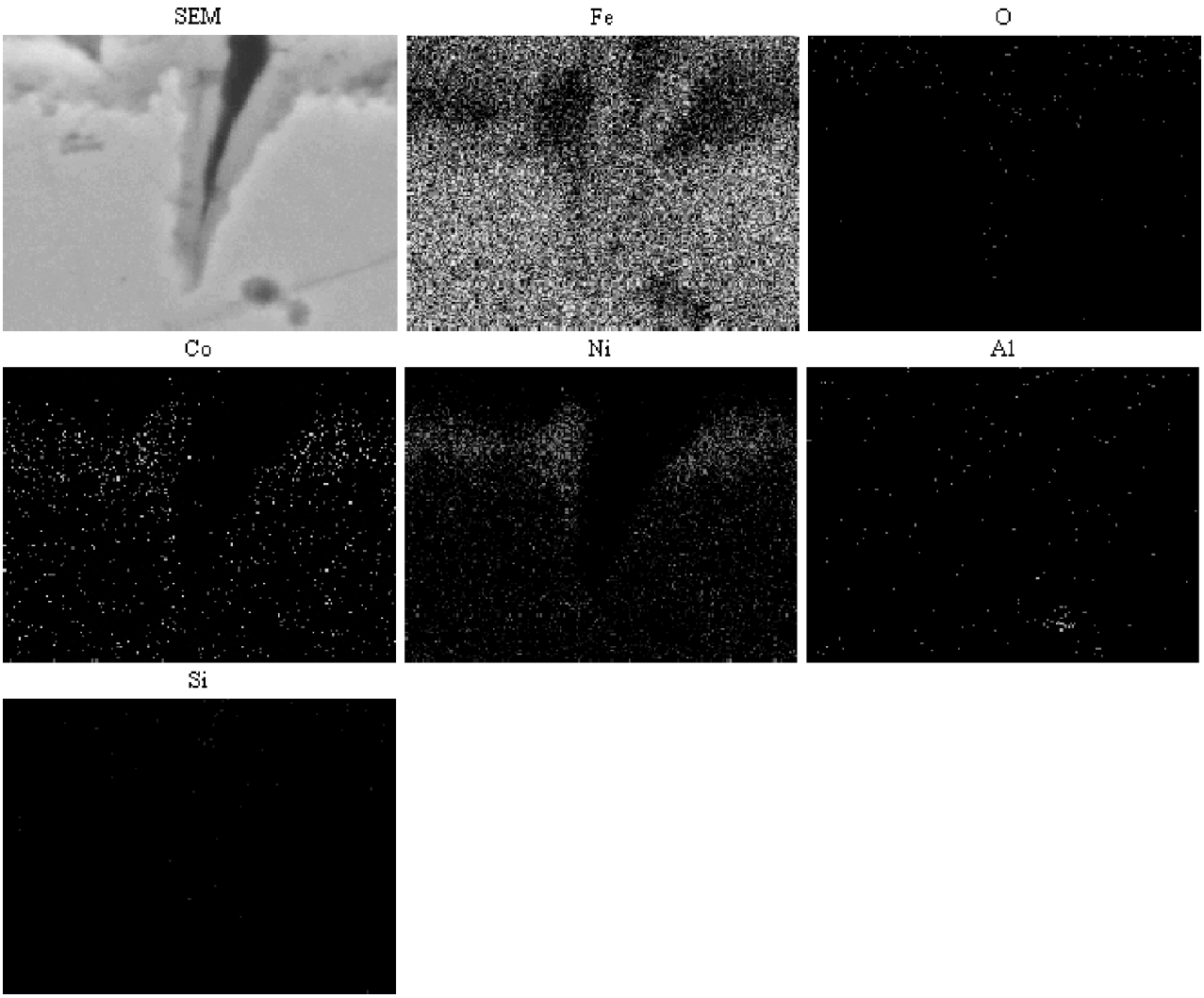

Slika 8: Kemična sestava jekla v okolici oksidnega klina, EDS (jeklo maraging)
Figure 8: Chemical composition of steel in the area oft the oxide wedge, EDS (maraging steel)

nadaljnjo rast pa polnjenje razpok s talino, oksidacija in popuščanje (prestaranje) jekla na površini.

4.2 Tvorba in rast razpok

Med vročo fazo cikla litja se na površini orodja pojavijo velike tlačne napetosti (**slika 2 b**), ki jih poveča tlak polnjenja gravure. Te napetosti sicer zavirajo nukleacijo in rast razpok, zato bi bile zaželene, vendar povzročajo lokalno plastično deformacijo. Le-ta je posebej izrazita na mestih, kjer so prisotni zarezni učinki, ostri prehodi ali velike spremembe mase orodja. V hladni fazi cikla se na površini orodja pojavijo velike natezne napetosti, ki so posledica plastične deformacije. Le-te pri temperaturi obratovanja presežejo kritično vrednost nosilnosti jekla. Pri cikličnem ponavljanju obremenitev nastane malociklično utrujanje, ki povzroča nastanek in rast razpok.

Rast razpok pospeši oksidacija površine jekla. Železovi atomi iz podpovršinskega sloja difundirajo na površino h kisiku, prazna mesta pa zapolnijo legirni elementi (**sliki 7 in 8**). Na površini orodja in razpoke se pojavi plast, sestavljena pretežno iz oksidov železa, tam pa so tudi oksidi aluminija in silicija, ki sta rezultat reakcije med kisikom in aluminijevo zlitino. Na meji med oksidno plastjo in jeklom (H13) se na zunanji strani nalagajo kromovi oksidi oz. oksidi kobalta in niklja pri jeklu maraging. Slabe strani oksidne plasti so nizka temperaturna razteznost, večji specifični volumen in krhkost. Oksidi in aluminijeve zlitine v razpokah povečajo natezne napetosti v klinu razpoke (med hladno fazo cikla), ki omogočajo rast razpok (**slika 7 b**) [5,19].

Natezne napetosti povzročajo lokalne razpoke v oksidni plasti in v polnilu razpoke (krhkost in razlika v temperaturni razteznosti) ter odpiranje razpok. Te v nadaljevanju delujejo kot kanali za dovajanje aluminijeve zlitine v razpoko in omogočajo penetracijo kisika do vrha razpoke, kjer povzročajo oksidacijo.

4.3 Rast razpok zaradi popuščanja (prestaranja) jekla

Orodja za tlačno litje aluminija, izdelana iz CrMoV orodnih jekel za delo v vročem, delujejo nad temperaturami sekundarnega utrjevanja [14]. Pri takih pogojih se skoraj v vseh jeklih pojavi nagnjenost k popuščanju jekla. Opazimo lahko tri stopnje mehčanja: (1) hitro mehčanje, kontrolirano z redukcijo dislokacij, (2) navidezno stacionarno mehčanje, ki ga vodi razvoj karbidov in (3) drastično zmanjšanje napetosti zaradi pojava velikih razpok [14]. Neželeno popuščanje jekla zmanjšuje napetost tečenja jekla in povzroča hitro napredovanje razpok do globine popuščene plasti. Popuščanje je posebej očitno pri jeklu H13, ki je imelo zaradi kaljena na zraku razogljičeno površino (**slika 5**). Slabše mehanske lastnosti te površine so povzročile rast razpok, kar je sprostilo napetosti v njihovi okolici ter s tem preprečilo nastanek novih razpok. Rast razpok preprečuje večja trdota (**sliki 5 in 6 a**), zato se je v jeklu H13, ki je bilo TO v vakuumu, pojavila večja gostota krajših razpok.

V navaru iz jekla maraging je trdota padla zaradi prestaranja med temperaturnim utrujanjem (**slika 5**). Krajše razpoke so se pojavile v nestaranem varu, ker pred preizkušanjem ni bil staran. Kljub temu pa toplotne obdelave staranja pri sanaciji orodij ne smemo izpustiti, saj s tem tvegamo pojav drugih poškodb zaradi premajhne trdote delovne površine.

Gostota temperaturnih razpok je v korelaciji z napetostjo tečenja jekla (**slika 6 b**), ki znaša za jeklo H13 1230 MPa, za jeklo maraging pa 1688 MPa [24,25]. V materialih z višjo napetostjo tečenja se pojavi večja gostota krajših razpok. Ker je trdota jekla v korelaciji z napetostjo tečenja bi pričakovali v jeklu maraging krajše razpoke oz. boljšo odpornost proti temperaturnemu utrujanju, če bi preprečili prestaranje jekla maraging med delom. Proti prestaranju so bolj odporna jekla maraging z manj Ni (od 10 % do 14 %).

Tabela 1: Toplotna obdelava epruvet iz jekla H13
Table 1: Heat treatment of H13 test specimens.

TO 1 – vakuum – kakovostna TO		TO 2 – brez zaščitne atmosfere – TO slabe kakovosti	
KALJENJE	1005 °C/35 min	KALJENJE	1000 °C/30 min
POPUŠČANJE 1	600 °C/150 min	POPUŠČANJE 1	530 °C/150 min
POPUŠČANJE 2	570 °C/240 min		

kaljenje = quenching, popuščanje = tempering, vakuum = vacuum, brez zaščitne atmosfere = without protective atmosphere

5 SKLEPI

V orodjih za tlačno litje neželeznih kovin je toplotno utrujanje glavni krivec za poškodbe. V vroči fazi cikla se na površini orodja pojavijo velike tlačne napetosti, ki jih dodatno zvišuje tlak polnjenja livne votline s talino. Na mestih hitrih in ostrih prehodov se pojavi plastična deformacija jekla. V hladni fazi cikla se na teh mestih pojavijo velike natezne napetosti, ki povzročijo nukleacijo razpok in rast s povečevanjem števila ciklov. Oksidacija površine orodja in površine razpok ter polnjenje razpok z aluminijevo talino povečajo natezne napetosti v klinu med hladno fazo in omogočajo rast razpok. V jeklih z večjo napetostjo tečenja in večjo trdoto se pojavi večje število krajših razpok, medtem ko se pri materialih z manjšo napetostjo tečenja in manjšo trdoto pojavi manjše število daljših razpok. Trajnost orodij za tlačno litje aluminijevih zlitin lahko podaljšamo z uporabo trdnejših, trdih in žilavih materialov, ki so bolj odporni proti popuščanju (staranje) med obratovanjem.

6 LITERATURA

[1] A. Srivastava, V. Joshi, R. Shivpuri, Computer modeling and prediction of thermal fatigue cracking in die-casting tooling, Wear 256 (**2004**), 38–43

[2] V. Joshi, K. Kulkarni, R. Shivpuri, R. S. Bhattacharya, S. J. Dikshit, D. Bhat, Dissolution and soldering behavior of nitrided hot working steel with multilayer LAFAD PVD coatings. Surface and Coatings Technology 146–147 (**2001**), 338–343

[3] V. Joshi, A. Srivastava, R. Shivpuri, Intermetallic formation and its relation to interface mass loss and tribology in die casting dies. Wear 256 (**2004**), 1232–1235

[4] A. Persson, S. Hogmark, J. Bergstrom, Simulation and evaluation of thermal fatigue cracking of hot work tool steels. International Journal of Fatigue 26 (**2004**), 1095–1107

[5] A. Persson, S. Hogmark, J. Bergstrom, Failure modes in field-tested brass die casting dies. Journal of Materials Processing Technology 148 (**2004**), 108–118

[6] A. Persson, S. Hogmark, J. Bergstrom, Thermal fatigue cracking of surface engineered hot work tool steels. Surface and Coatings Technology 191 (**2005**), 216–227

[7] Young, W.: Why Die Casting Dies Fail, Paper No. G-T79-092, (**1979**), 1-7. St.Louis, Missouri, NADCA. 10th SDCE International die casting exposition & congress

[8] Y. Wang, A study of PVD coatings and die materials for extended die-casting die life. Surf. and Coat. Techn. 94–95 (**1997**), 60–63

[9] K. Kulkarni in sod., Thermal cracking behavior of multi-layer LAFAD coatings on nitrided die steels in liquid aluminum processing. Surf. and Coat. Techn. 149 (**2002**), 171–178

[10] P. Panjan in sod., Improvement of die-casting tools with duplex treatment. Surface and Coatings Technology 180–181 (**2004**), 561–565

[11] Marlok, Longer die life Better quality, www.metsopowdermet.com (**2005**). Metso Powdermet.

[12] Fuchs, K. D.: Hot-work tool steels with improved properties for die casting applications, Rosso, M., Actis Grande, M, in Ugues, D. II, (**2006**). 17–26. Torino, Proceedings of 7th International Tooling Conference

[13] Ahmer, Z. in sod., Cyclic behaviour simulation of X38CrMoV5-47HRC (AISI H11) tempered martensitic hot work tool steel, Rosso, M., Actis Grande, M, in Ugues, D. II, (**2006**). 513–520. Torino, Proceedings of 7th International Tooling Conference

[14] Bergström, J., F. Rézai-Aria.: High temperature fatigue of tool steels, Rosso, M., Actis Grande, M, in Ugues, D. II, (**2006**), 545–554. Torino, Proceedings of 7th International Tooling Conference

[15] Michaud, P. in sod., Influence of chemical composition on the precipitation of secondary carbides in modified AISI H11 hot-work tool steels, Rosso, M., Actis Grande, M, Ugues, D. (**2006**), 733–740. Torino, Proceedings of 7th International Tooling Conference

[16] Daffos, C., P. Lamesle, F. Rézai-Aria.: Fatigue-oxidation interaction models for life prediction of hot foeming tools steels under transient thermomechanical loadings, Rosso, M., Actis Grande, M, in Ugues, D. II, (**2006**), 471–478. Torino, Proceedings of 7th International Tooling Conference

[17] Medjedoub, F. in sod., Experimental conditions and enviromental effects on thermal fatigue damage accumulation and life of die-casting steel X38CrMoV5 (AISI H11), Rosso, M., Actis Grande, M, in Ugues, D. II, (**2006**), 461–470. Torino, Proceedings of 7th International Tooling Conference

[18] B. Kosec, L. Kosec, J. Kopač, Analysis of casting die failures. Engineering Failure Analysis 8 (**2001**), 355–359

[19] F. Kosel, L. Kosec, Heat checking of hot work tools. Mechanical Engineering Journal 29, (**1983**), E1-E8

[20] J. F. Wallace, D. Schwam, Development Studies on Selection and processing of Die Materials to Extend Die Life, Die Casting Engineer, (**2000**), 50–58

[21] Klobčar, D., J. Tusek, B. Taljat, G. Scavino.: Influence of thermal fatique on materials for die-casting tooling, Rosso, M., Actis Grande, M., Ugues, D. (2-5-2006). 479–485. Torino, Proceedings of 7th International Tooling Conference

[22] D. Klobčar, J. Tušek, B. Taljat, Thermal fatigue of materials for die-casting tooling. MSEA (**2007**)

[23] Abaqus 6.4, (**2003**), Hibbit, Karlsson & Sorensen, Inc.

[24] Materialne lastnosti jekla H13, www.sz-metal.si, (**2003**), 6-9-2003

[25] QRO 90 Supreme, Hot work tool steel, Tool steel facts, www.uddeholm.com, Uddeholm. 15.9.2005

UDK 621.791:669.715
Izvirni znanstveni članek/Original scientific article

ISSN 1580-2949
MTAEC9, 42(5)211(2008)

LASERSKO REPARATURNO VARJENJE TERMORAZPOK NA ORODJIH ZA TLAČNO LITJE ALUMINIJA

LASER REPAIR WELDING OF THERMAL CRACKS ON ALUMINIUM DIE CASTING DIES

Matej Pleterski[1], Janez Tušek[1], Ladislav Kosec[3], Damjan Klobčar[1], Mitja Muhič[2], Tadej Muhič[2]

[1]Univerza v Ljubljani, Fakulteta za strojništvo, Aškerčeva 6, 1000 Ljubljana
[2]TKC, d. o. o., Trnovska 8, 1000 Ljubljana
[3]Univerza v Ljubljani, Naravoslovnotehniška fakulteta, Aškerčeva 12, 1000 Ljubljana

Prejem rokopisa – received: 2007-09-20; sprejem za objavo – accepted for publication: 2008-07-02

Sanacija poškodovanih in izrabljenih orodij je ukrep, s katerim lahko v veliki meri povečamo produktivnost in zmanjšamo proizvodne stroške. Zato se v zadnjem času vedno več uporablja laserska tehnologija, katere prednost je predvsem v ozkem lokalnem delovanju toplotne energije, majhni toplotno vplivani coni in zanemarljivih obrobnih zajedah. Orodja za tlačno litje so med delovanjem izpostavljena kompleksnim termomehanskim obremenitvam in s tem visokim napetostim na površini, ki povzročijo utrujanje materiala in nastanek razpok. V članku je predstavljena tehnologija sanacije razpok (žlebljenje, varjenje) z bliskovnim Nd:YAG-laserjem, vključno z analizo mikrotrdot ob sami razpoki, žlebu in varu. Rezultati kažejo na to, da je z laserjem mogoče relativno hitro in enostavno odstraniti utrujeno območje ob razpoki, ga navariti ter tako orodje usposobiti za obratovanje.

Ključne besede: tlačno litje, orodja, razpoke, poprava, lasersko navarjanje, aluminij

Repair welding of damaged and worn-out tools is a measure, which can increase productivity and lower production costs to a great extent. For this purpose, laser technology has recently been used with major benefits such as localized heating effect, narrow heat effected zone and negligible undercuts. In the die-casting process, dies are submitted to a complex thermo mechanical stressing and high stresses on the surfaces of dies are induced. That may lead to thermal fatigue cracking. In this paper, the technology of thermal cracks repair (grooving, welding) with pulsed Nd:YAG laser is described. A micro-hardness analysis of areas surrounding cracks, grooves and welds has been performed, also. The test results suggest that it is relatively fast and easy to eliminate the fatigue area surrounding the cracks, and with proper welding to reestablish the tool operability.

Key words: die casting, dies, cracks, repairing, laser welding, aluminium

1 UVOD

Lasersko varjenje je ena izmed prvih industrijskih aplikacij laserja. Ta alternativna tehnologija daje nove možnosti obdelave, dodelave in sanacije, kjer je varjenje z drugimi varilskimi metodami oteženo ali celo onemogočeno. V to vrsto laserske obdelave spada tudi lasersko reparaturno zvarjanje in navarjanje, ki je relativno nova tehnologija in se vedno bolj uveljavlja v livarski, orodjarski ter drugi strojni industriji za sanacijo in vzdrževanje orodij. Orodja za tlačno litje so izdelana iz kakovostnih jekel za delo v vročem, ki so dobro odporna proti toplotnim deformacijam, šokom ter termičnim razpokam na površini. Ena izmed najpomembnejših karakteristik orodja je trdota. Pri orodjih za tlačno litje barvnih kovin mora biti le-ta okoli *HRc* = 45. Za povečanje trajnostne dobe jih lahko še nitriramo in s tem povečamo njihovo površinsko odpornost proti obrabi. Orodja so med uporabo izpostavljena kompleksnim termomehanskim obremenitvam in s tem visokim napetostim na površini, ki povzročijo utrujanje materiala ter nastanek razpok na površini, ne glede na vrsto materiala, toplotno obdelavo in vrsto oplemenitenja površine orodja. Na **sliki 1** je prikazana tipična termična razpoka, ki se močno izraža tudi na odlitku. Takšni odlitki so nesprejemljivi, zato je treba orodja med obratovalno dobo sanirati. Zato so se navadno uporabljali procesi, kot so brušenje, rezkanje in obločno varjenje. Z laserjem je mogoče razpoko izžlebiti, pa tudi

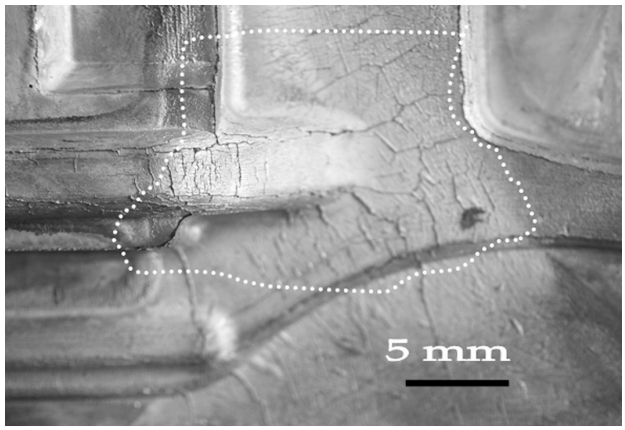

Slika 1: Odtisi temen razpok zaradi termičnega razpokanja na ulitku
Figure 1: Imprints of cracks on a cast, as a result of thermal cracking

zavariti. Sun in sod. [1,2] so napravili študiji o trajnodinamični in natezni trdnosti ter žilavosti po pretaljevanju razpok, ki so nastale pri trajni dinamični obremenitvi pri povišanih temperaturah. Treba je poudariti, da je šlo pri obeh njihovih raziskavah zgolj za pretaljevanje razpok brez dodajanja materiala. Vedani in sod. [3] so opravili študijo s poudarkom na razvoju mikrostuktur in metalurških problemih pri reparaturnem varjenju površinsko obdelanih orodnih jekel. Nekateri avtorji [4,5] so raziskovali lasersko reparaturno varjenje na različnih področjih. Brown in sod. domnevajo, da je lasersko reparaturno varjenje razpok na ladijskih pločevinah bolj učinkovito kot varjenje z obločnimi postopki zaradi krajših časov in nižjih stroškov.

2 EKSPERIMENTALNI DEL

Eksperimenti so bili izvedeni na obrabljenem stranskem jedru orodja za tlačno litje koluta za navijanje varnostnega pasu v avtu, vzdolž katerega je potekala razpoka. Orodje iz materiala 1.2343 (X38CrMoV5-1), kaljeno na trdoto 45 ± 2 HRc (450 ± 30 HV) je prikazano na **sliki 2**. Orodje je bilo na začetku odrezano na rezu 1. Ta kos se je rabil za analizo trdote ob razpoki. Razpoko na preostalem delu orodja se je nato požlebilo z bliskovnim Nd:YAG-laserjem moči 120 W. Po žlebljenju je bilo orodje odrezano na rezu 2. Drugi kos se je rabil za analizo trdote ob žlebu. Preostanek orodja je bil nato zavarjen z dodajnim materialom Uddeholm G3 premera 0,5 mm in odrezan na rezu 3. Uporabljeni parametri za žlebljenje in varjenje so prikazani v **tabeli 1**. Pri izžlebljenju z laserskim žarkom je treba izbrati parametre z visoko gostoto energije v gorišču laserskega žarka. Material, tj. jeklo, je bilo treba upariti in ga odstraniti iz razpoke. Za žlebljenje je zahtevana gostota energije več kot 10^{10} W/m^2. To se doseže z nastavitvijo visoke moči na laserskem izvoru in izbiro leče s kratko goriščno razdaljo. Parametri za varjenje morajo biti prilagojeni predvsem velikosti izžlebljenega utora in premeru uporabljene žice. V obeh primerih je bil kot zaščitni plin uporabljen Ar čistote 99,9996 %. Iz odrezanih delov orodja so bili napravljeni makroobrusi, na katerih so bile nato opravljene meritve mikrotrdot po Vickersu pri obremenitvi 100 g oz. sili 0,981 N. Vsi vzorci so bili jedkani z nitalom (4 %). Meritve so bile opravljene na treh globinah orodja: (0,3, 0,6 in 1) mm. Zaradi boljše preglednosti so v nadaljevanju predstavljene zgolj meritve trdot na globini 1 mm.

Tabela 1: Prikaz nastavitvenih parametrov pri laserskem žlebljenju in varjenju razpok
Table 1: Parameters for laser grooving and welding

Parameter	Žlebljenje	Varjenje
Frekvenca las. bliskov y /Hz	6	7,4
Čas trajanja las. bliska t_p /ms	6,2	6,2
Povprečna moč las. bliska P_{pp} /W	900	400
Povp. energija las. bliska E_p /J	15,3	11,9
Goriščna razdalja leče f_l /mm	160	200

3 REZULTATI IN DISKUSIJA

Na **sliki 3** je prikazan makroobrus razpoke. Z meritvami trdote, prikazanimi na **sliki 4 a**, smo ugotovili, da je trdota okoli razpoke višja, kar je razvidno tudi iz diagrama na **sliki 4 b**, kjer je trdota ob razpoki v povprečju za *HV* = 200 višja od normalne trdote orodja. To sicer ni značilno za področja ob termičnih razpokah, tako da lahko sklepamo, da je bilo to orodje pred našo analizo verjetno že sanirano. Navadno trdota materiala ob neposredni bližini termične razpoke rahlo pade, kar je posledica kemijske nehomogenosti jekla v območju ob površini razpoke. Železovi atomi iz sloja pod površino razpoke difundirajo na površino proti kisiku, na prazna mesta pa difundirajo legirni elementi (Cr, Mo, V). Na površini razpoke se tako pojavi plast, ki je v veliki meri sestavljena iz železovih oksidov in oksidov aluminija in silicija, kar je posledica reakcije aluminijeve zlitine in kisika. Na meji te oksidne plasti in osnovnega materiala pa se kopičijo predvsem oksidi kroma. Slaba stran oksidne plasti je nizka temperaturna razteznost, večji volumen in krhkost. Oksidi in aluminijeve zlitine v razpokah povečajo natezne napetosti v klinu razpoke, kar povzroča njihovo rast [6]. Razpoke v nadaljevanju delujejo kot kanali za dovajanje aluminijeve zlitine v razpoko in

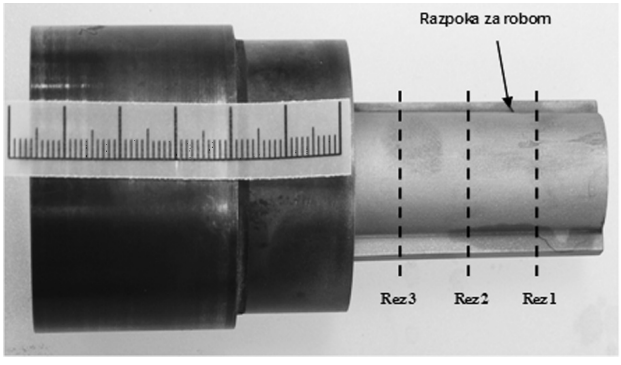

Slika 2: Stransko jedro z označenimi področji razreza
Figure 2: Test specimen with marked cuts

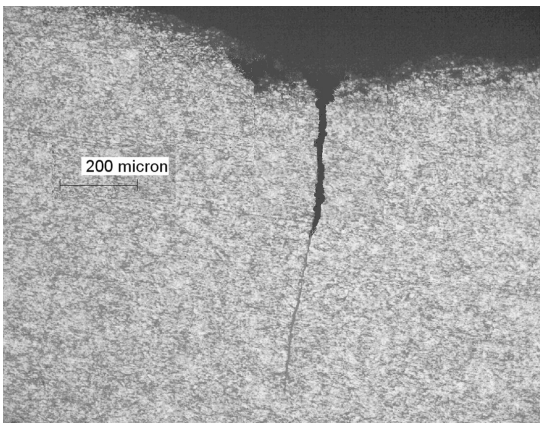

Slika 3: Makroskopska slika termične razpoke
Figure 3: Macro section of a thermal crack

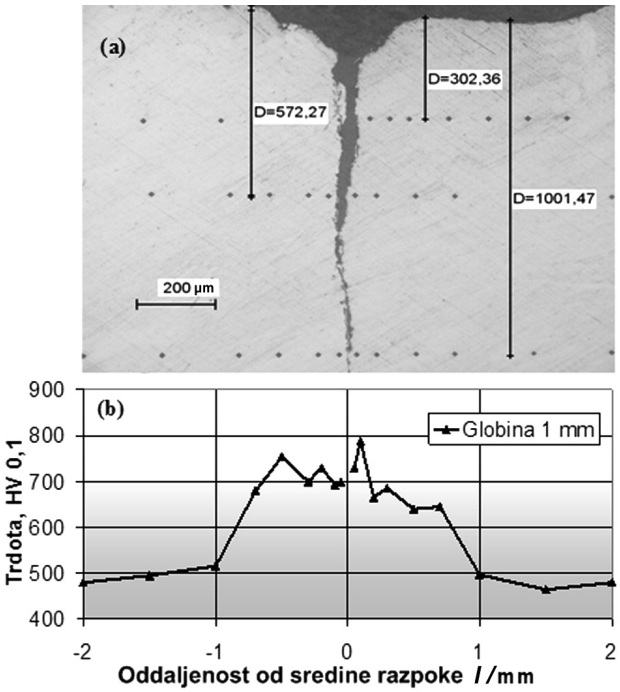

Slika 4: Merilna mesta (a) in profil trdote pravokotno na razpoko (b)
Figure 4: Location of measurements (a) and the hardness profile in direction perpendicular to the crack (b)

omogočajo penetracijo kisika do konice razpoke, kjer povzroči oksidacijo. Pri nadaljnjem obratovanju takega orodja se razpoka še hitreje širi, postaja vedno globlja in širša. Vse skupaj vodi do nesprejemljivih ulitkov, orodje pa lahko pri nadaljnjem obratovanju v takem stanju poči po celotni globini. Tako poškodovana orodja se navadno sanirajo (če je sanacija sploh še stroškovno upravičena) z rezkanjem razpoke in varjenjem po postopku TIG s predgrevanjem, zajede pa se nato popravijo z laserjem. Pri takšni sanaciji je treba veliko mehanske in toplotne obdelave.

Na **sliki 5** je prikazan makroobrus izžlebljene razpoke, na katerem je lepo vidno toplotno vplivano področje in tisto, ki je bilo med žlebljenjem pretaljeno in ponovno zakaljeno (svetel rob tik ob žlebu). Ta, pri-

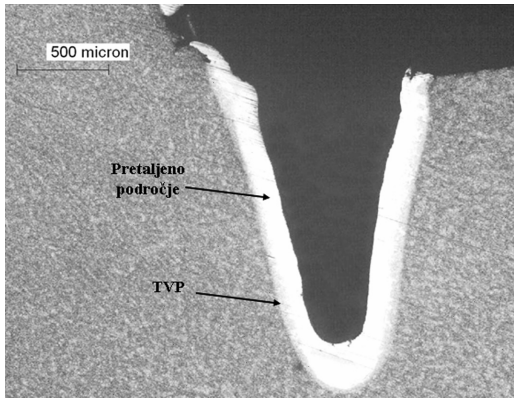

Slika 5: Makroskopska slika izžlebljene razpoke
Figure 5: Macro section of the groove

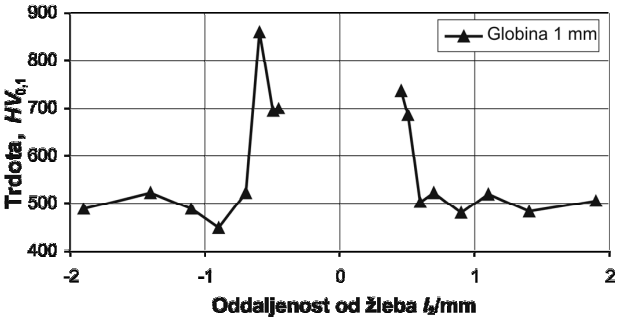

Slika 6: Profil trdote ob zvarnem žlebu
Slika 6: Hardness profile in the direction perpendicular to the groove

bližno 0,2 mm širok pas se izraža tudi v diagramu meritev trdot, ki je prikazan na **sliki 6**. Trdote so v tem pasu tudi do *HV* = 300 večje od normalne trdote orodja (izstopajoča meritev, ki sega nad *HV* = 850, je posledica kemične nehomogenosti jekla v tem območju). Iz diagrama je tudi razvidno, da trdota z oddaljenostjo od zvarnega žlebu naglo pada in po 0,2 mm do 0,3 mm doseže normalno trdoto orodja. Razlog za tako visoke trdote je predvsem v relativno veliki gostoti vnesene energije, kar je pogoj za uspešno žlebljenje območja ob razpoki. Ker se orodja v primeru laserskega reparaturnega varjenja varijo v hladnem, se segreti material in talina, ki se ne odstrani iz žleba, znova zakalita. Zaradi velikega temperaturnega gradienta med tem območjem, segretim nad temperaturo tališča jekla, in osnovnim materialom (sobna temperatura) se to območje izredno hitro ohladi in s tem močno zakali. Mikrostruktura, ki nastane v takem primeru, je prikazana na SEM-posnetku na **sliki 7**.

Na **sliki 8** je prikazan makroobrus zavarjene razpoke. Meritve trdot na varu so prikazane v diagramu **slike 9**. Eden izmed ciljev pri reparaturnem varjenju je, da se doseže trdota zvara čim bolj enaka trdoti osnovnega materiala. Na to pa lahko vplivamo predvsem z izbiro

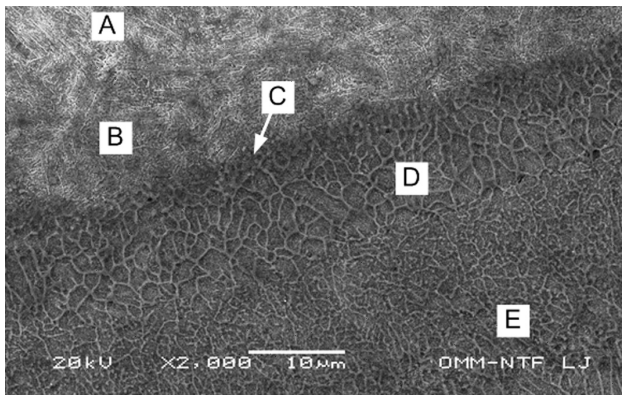

Slika 7: Mikrostruktura jekla ob zvarnem žlebu (Sl. 5): A-osnovni material; B-TVP; C-meja nataljevanja; D-območje celične mikrostrukture, E-območje aksialnih dendritov; SEM (SEI)
Figure 7: Image of microstructure at the groove: A-base material; B-HAZ; C-solidification line; D-cellular dendrite area; E-axial dendrite area; SEM (SEI)

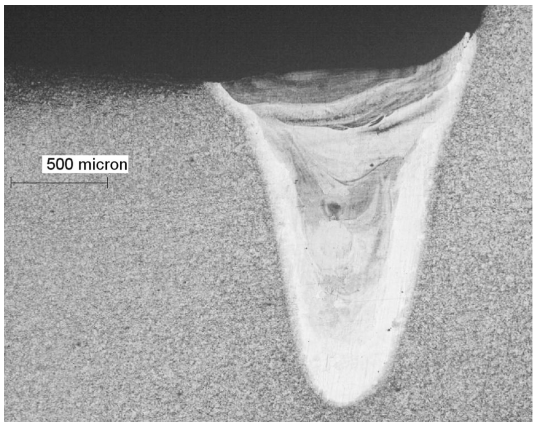

Slika 8: Makroskopska slika navarjenega zvarnega žleba
Figure 8: Macro section of the welded groove

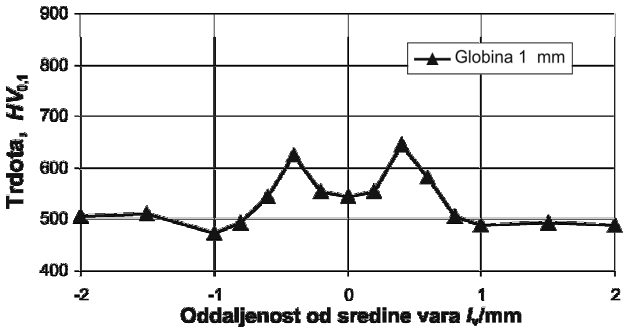

Slika 9: Profil trdote preko zvara
Figure 9: Hardness profile across the weld

primernega dodajnega materiala in varilnimi parametri. Zaradi majhne količine taline in velikega gradienta temperature uporabljamo pri laserskem reparaturnem varjenju dodajne materiale, ki imajo znižan delež C (0,2 %) in zvišano vsebnost Cr (1,5 %) in Mo (3 %) glede na osnovni material. Prav tako moramo biti pazljivi pri nastavitvi parametrov, da vnesena energija ni prevelika, vendar še tolikšna, da se dodajni material pretali in v celoti zlije z osnovnim. **Na sliki 10** je prikazan SEM-posnetek območja na robu zvara, ki je z mešano celično-dendritno mikrostrukturo podobno tistemu ob zvarnem žlebu, zato so tudi trdote v tem prehodnem področju visoke. Mikrostruktura v sredini vara pa je prikazana na **sliki 11**. Gre za martenzitno mikrostrukturo z redkejšimi neizrazitimi dendriti in trdoto rahlo višjo od osnovnega materiala.

4 SKLEPI

Rezultati raziskave kažejo, da je z lasersko tehnologijo mogoče relativno hitro in enostavno sanirati razpokano orodje. Z ustreznimi parametri laserskega žarka je mogoče razpoko izžlebiti ter tako odstraniti utrujeni material ob razpoki. Čeprav se ob tako pripravljenem

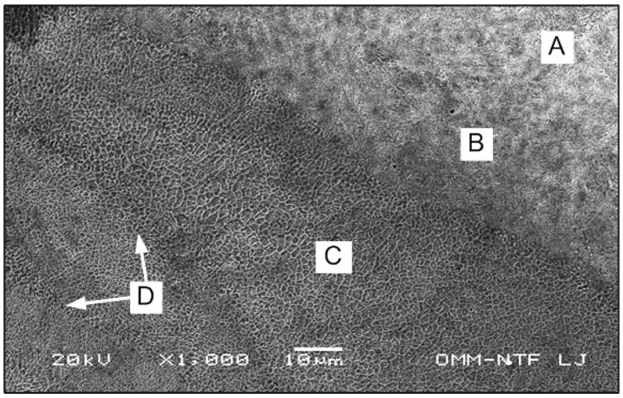

Slika 10: Mikrostruktura jekla na robu zvara: A-osnovni material; B-TVP; C-območje celično-dendritne mikrostrukture; D-pasovi toplotnega vpliva zaradi večvarkovnega polnjenja žleba; SEM (SEI)
Figure 10: Microstructure at the weld boundary: A-base material; B-HAZ; C- dendrite area; D-layers of heat effect of multi-pass groove filling; SEM (SEI)

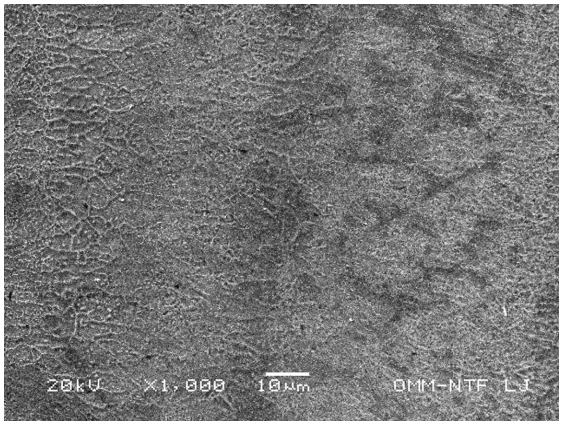

Slika 11: Mikrostruktura v varu; fina dendritna mikrostruktura; SEM (SEI)
Figure 11: Microstructure in the weld; Fine dendritic microstructure; SEM (SEI)

žlebu pojavi ozko pretaljeno področje, ki se močno zakali, je mogoče ob nastavitvi primernih laserskih parametrov in izbiri pravega dodajnega materiala orodje zvariti tako, da je trdota zvara blizu trdoti osnovnega materiala.

5 LITERATURA

[1] Y. Sun, S. Hanaki, M. Yamashita, H. Uchida, H. Tsujii: Vacuum 73 (**2004**), 655–660
[2] Y. Sun, H. Sunada, N. Tsujii: ISIJ International, 41 (**2001**) 9, 1006–1009
[3] M. Vedani: Journal of Materials Science (**2004**), 241–249
[4] E. Capello, D. Colombo, B. Previtali: Journal of Materials Processing Technology 164–165 (**2005**), 990–1000
[5] P. M. Brown, G. Shannon, W. Deans, J. Berd: Weld World (**1999**), 33
[6] F. Kosel, L. Kosec: Mechanical Engineering Journal 29, (1983), E1-E8

UDK 669.715:620.17.112
Original scientific article/Izvirni znanstveni članek

ISSN 1580-2949
MTAEC9, 42(5)215(2008)

USE OF ARTIFICIAL NEURAL NETWORKS IN BALL BURNISHING PROCESS FOR THE PREDICTION OF SURFACE ROUGHNESS OF AA 7075 ALUMINUM ALLOY

UPORABA UMETNIH NEVRONSKIH MREŽ ZA NAPOVED HRAPAVOSTI POVRŠINE PRI KROGELNEM GLAJENJU ALUMINIJEVE ZLITINE AA 7075

Ugur Esme[1], Aysun Sagbas[2], Funda Kahraman[3], M. Kemal Kulekci[4]

Mersin University, Tarsus Technical Education Faculty, Department of Mechanical Education, 33400, Tarsus-Mersin/Turkey
uesme2003@hotmail.com

Prejem rokopisa – received: 2008-06-25; sprejem za objavo – accepted for publication: 2008-07-09

Burnishing is a plastic deformation process, and it has become more popular as a finishing process. Thus, it is especially crucial to select the burnishing parameters to reduce the surface roughness. In the present study, a surface roughness prediction model using artificial neural network (ANN) is developed to investigate the effects of burnishing conditions during machining of AA 7075 aluminum material. The ANN model of surface roughness parameters (R_a) is developed considering the conditions as burnishing force, number of tool passes, feed rate and burnishing speed. The experimental results were trained in an ANN program and the results were compared with experimental values. It is observed that the experimental results coincided with ANN results.

Keywords: Ball burnishing, surface roughness, modeling, artificial neural network

Glajenje je proces plastične deformacije in je postalo zelo razširjeno kot končna obdelava. Za zmanjšanje hrapavosti površine je zelo je pomembna izbira parametrov glajenja.V tej raziskavi je bil z uporabo nevronske mreže (ANN) razvit model glajenja pri obdelavi aluminijeve zlitine AA 7075. Model parametra hrapavosti površine (R_a) je bil razvit z upoštevanjem pogojev: polirna sila, število prehodov orodja, hitrost podajanja in hitrost poliranja. Eksperimentalni podatki so uporabljeni za ANN-program, rezultati modela pa primerjani z eksperimentalnimi. Rezultati ANN se dobro ujemajo z eksperimentalnimi.

Ključne besede: krogelno glajenje, hrapavost površine, modeliranje, umetna nevronska mreža

1 INTRODUCTION

The surface quality is an important parameter to evaluate the productivity of machine tools as well as machined components. Hence, achieving the desired surface quality is of great importance for the functional behavior of mechanical parts [1]. Surface roughness is used as the critical quality indicator for the machined surfaces and since, it affects several properties such as wear resistance, fatigue strength, coefficient of friction, lubrication, wear rate and corrosion resistance of the machined parts [2]. In today's manufacturing industry, special attention is given to dimensional accuracy and surface finish. Thus, measuring and characterizing the surface finish can be considered as a predictor for the machining performance.

Burnishing is considered as a cold-working finishing process differing from other cold-working surface treatment processes such as shot peening and sand blasting, etc. in that it produces a good surface finish and also induces residual compressive stresses at the metallic surface layers [3,4]. Accordingly, the burnishing is distinguished from chip-forming finishing processes such as grinding, honing, lapping and super-finishing which induce residual tensile stresses at the machined surface layers [5]. Also, burnishing is economically desirable, because it is a simple and cheap process, requiring less time and skill to obtain a high-quality surface finish [6]. The burnishing process can be achieved by applying a highly polished and hard ball or roller onto a metallic surface under pressure. As indicated in **Figure 1**, pressure causes the peaks of the metallic surface to spread out permanently and fill the valleys [4], when the applied burnishing pressure exceeds the yield strength of the metallic material.

The surface of the metallic material will be smoothed out and because of the plastic deformation the surface is

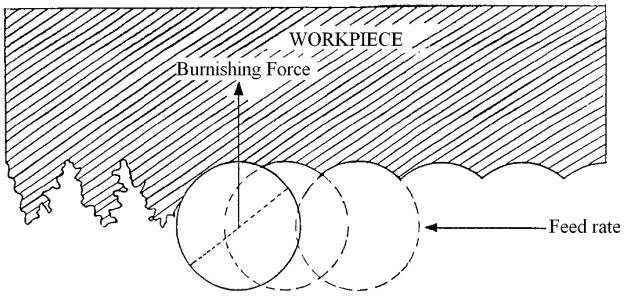

Figure 1: Schematic representation of ball burnishing process [7]
Slika 1: Shematska predstavitev procesa krogelnega poliranja [7]

work hardened and the material is left with a residual stress distribution compressive on the surface [4]. The changes in surface characteristics due to burnishing will cause improvements in surface hardness, wear resistance, fatigue resistance, yield and tensile strength and corrosion resistance, as claimed by many authors [8–11].

The aim of the present work was to investigate the effect of burnishing parameters such as burnishing force (F/N), number of tool passes (N), feed rate (f/(mm/min)) and burnishing speed (v/(r/min)) on the surface roughness (R_a/μm) of AA 7075 aluminum with the use of ANN.

2 MATERIAL AND EXPERIMENTAL PROCEDURE

2.1 Material

In this study, high strength precipitation hardening 7XXX series wrought aluminum alloy AA 7075 was used. The strength and good mechanical properties make the AA 7075 aluminum alloy appropriatefor use in aerospace industry. The chemical composition and mechanical properties of the workpiece material is given in **Table 1**.

Table 1: Chemical and mechanical properties of workpiece material
Tabela 1: Sestava in mehanske značilnosti obdelovanca

Chemical composition *w*/%	Al	Cu	Mg	Cr	Zn
	90.0	1.60	2.50	0.23	5.60
Mechanical properties	Tensile strength (MPa)	Yield strength (MPa)	Shear strength (MPa)	Fatique strength (MPa)	Hardness (HB 500)
	220	95	150	160	60

The three part workpiece material shown in **Figure 2**, was prepared with the dimensions of 30 mm diameter and 60 mm in length with each segment with 20 mm in length.

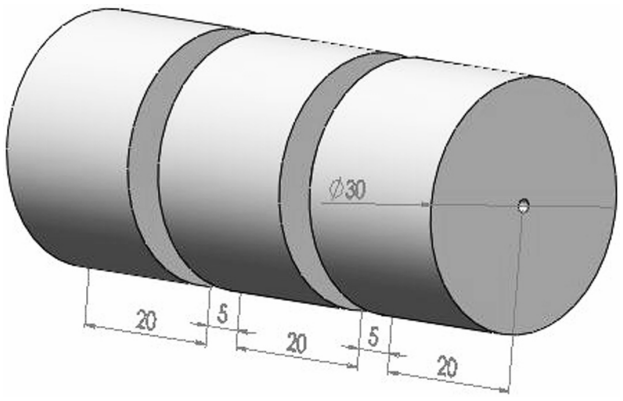

Figure 2: Dimensions of workpiece material
Slika 2: Mere obdelovanca

2.2 Machines and Equipments

A 18 mm diameter steel ball was used for burnishing. The detailed drawing is shown in **Figure 3**. When the ball or roller is pressed against the surface of the metallic specimen, a pre-calibrated spring was compressed used mainly to reduce the possible sticking of the tool onto the surface.

The experiments were performed on a FANUC GT-250B CNC machining center. The burnishing tool was mounted on the CNC turret as shown in **Figure 4**.

Dry turning and burnishing were used in all the experimental work and alcohol was used to clean the specimens before burnishing. The cleaning of the ball was carried out continuously in order to prevent any hard particles from entering the contact surface between the tool and the specimen, such hard particles usually leaving deep scratches that may damage the burnished surface of the specimen. The Phynix TR-100 model surface roughness tester was used to measure the surface roughness of the burnished samples. Cut off length was chosen as 0.3 for each roughness measurement. Six measurements of surface roughness were taken from the samples and average of the roughness was used in modeling.

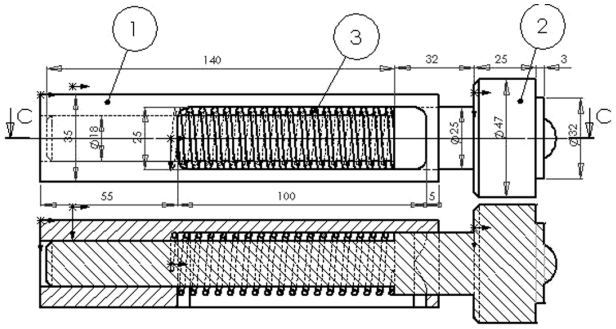

Figure 3: Detailed drawing of the ball burnishing tool: (1) casing; (2) adapter cover; (3) spring
Slika 3: Načrt orodja za krogelno glajenja. (1) ohišje, (2) prilagoditveni pokrov, (3) vzmet

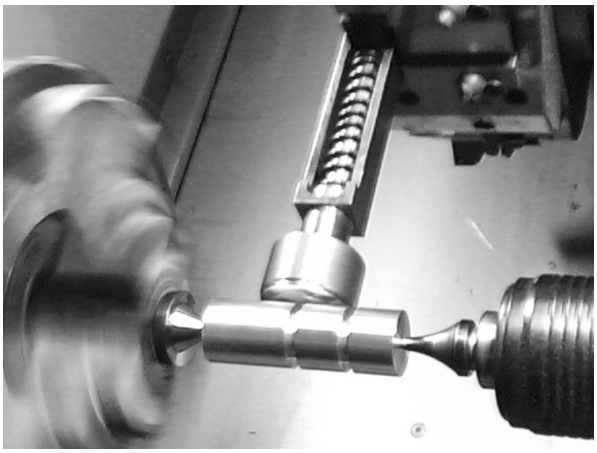

Figure 4: Ball burnishing experimental set up
Slika 4: Eksperimentalna priprava za krogelno glajenje

3 MODELING WITH ARTIFICIAL NEURAL NETWORK (ANN)

Computers are an integral part of day to day activities in engineering design and engineers have utilized various applications to assist them improve their design [12]. ANN mimics some basic aspects of the brain functions [13–15]. It is based on the neural structure of the human brain, which processes information by means of interaction between many neurons [13,16]. In the past few years there has been a constant increase in interest of neural network modeling in different fields of materials science. The basic unit in the ANN is the neuron. The neurons are connected to each other with weight factor. A network is usually trained using a large number of input with corresponding output data [17].

The ANN architecture used modeling of surface roughness is illustrated in **Figure 5**. It consists of many simple processing neurons organized in a sequence of layers: input, intermediate (hidden) and output layers. The simulation problem consists of finding a satisfactory relationship between a set of neurons representing the input data and associated known output. The selection of the input parameters is a very important aspect of neural network modeling [17]. All relevant input parameters must be represented as the input data of the neural network. In this study burnishing force, number of passes, feed and burnishing speed were used as inputs while surface roughness was used as an output.

The ANN model used is 4 : 5 : 5 : 1 multilayer architecture as shown in **Figure 5**. Y_j (j = 1, 2,..,5) and Y_i (i = 1, 2,..,5) are the output of the hidden neurons.

3.1 The Training of the Network

Generally, there are three different learning strategies. First, the trainer may tell the network what it should learn (Supervised Learning), second, the trainer may indicate whether or not the output is correct without telling what the network should learn (Reinforcement Learning) and finally, the network learns without any intervention of the trainer (Unsupervised Learning). The learning set consists of the inputs and the outputs used in training the network. The required outputs take place in this set in the case of supervised learning, while in other cases, they are not found in it [17,18]. In the present study, the supervised learning approach was used. The computer program has been developed under MATLAB [19]

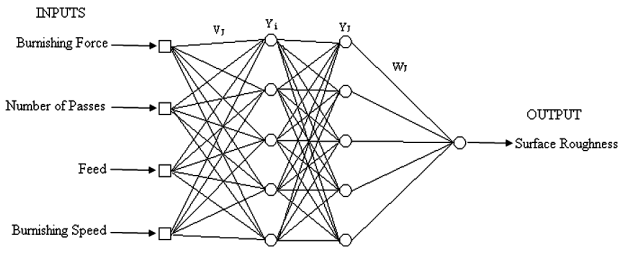

Figure 5: The constructed ANN model
Slika 5: Razviti ANN-model

and as given in **Table 2**, a database of 30 experimental results was used to train the ANN model.

Table 2: Experimental results and training set of ANN modeling
Tabela 2: Eksperimentalni rezultati in učni podatki za ANN-modeliranje

Exp.no	Burnishing force F/(9,86 N)	Number of passes N	Feed rate f/(mm/min)	Burnishing speed v/(r/min)	Measured surface roughness R_a/μm
1	9	2	0.62	200	0.30
2	10	3	0.80	400	0.37
3	11	2	0.60	500	0.37
4	12	3	0.45	800	0.47
5	13	2	0.45	1000	0.44
6	14	4	0.45	600	0.65
7	15	4	0.45	600	0.71
8	16	2	0.27	200	0.60
9	17	3	0.62	600	0.69
10	18	4	0.45	600	0.89
11	19	3	0.27	400	0.85
12	20	2	0.27	500	0.78
13	21	3	0.45	600	0.91
14	22	4	0.27	1000	1.12
15	23	2	0.62	700	0.75
16	24	3	0.45	600	1.06
17	25	2	0.27	200	1.02
18	9	4	0.27	200	0.38
19	10	2	0.62	300	0.33
20	12	4	0.45	400	0.54
21	16	3	0.80	500	0.63
22	13	3	0.60	600	0.51
23	15	2	0.27	700	0.55
24	16	3	0.62	800	0.64
25	17	4	0.45	900	0.82
26	20	3	0.62	1000	0.81
27	14	2	0.45	400	0.49
28	16	4	0.80	600	0.76
29	11	3	0.27	800	0.42
30	10	2	0.45	800	0.33

3.2 Testing Stage

In order to understand whether an ANN is making good predictions, test data that has never been presented to the network are used and the results are checked at this stage. The statistical methods of root mean square error (RMSE), the coefficient of multiple determination (R^2) values have been used for making comparisons [17,20–23]. These values are determined by the following equations:

$$RMSE = \left(\frac{1}{n} \sum_j \left| a_j - p_j \right|^2 \right)^{1/2} \quad (1)$$

$$R^2 = 1 - \left(\frac{\sum_j \left(a_j - p_j \right)^2}{\sum_j \left(p_j \right)^2} \right) \quad (2)$$

Table 3: Validation set used for ANN analysis
Tabela 3: Podatki za preverjanje ANN-analize

Exp.no	Burnishing force F/(9,81 N)	Number of passes N	Feed rate f/(mm/min)	Burnishing speed v/(r/min)	Measured surface roughness R_a/μm	*ANN*			
						Predicted surface roughness R_{ap}/μm	Error %	*RMSE*	R^2
1	10	2	0.62	200	0.34	0.36	-6.75	0.0051	0.9960
2	10	3	0.80	600	0.36	0.38	-4.23	0.0034	0.9984
3	11	4	0.27	200	0.50	0.52	-4.42	0.0049	0.9982
4	12	3	0.45	400	0.47	0.45	5.22	0.0055	0.9970
5	13	3	0.45	1000	0.49	0.48	1.91	0.0021	0.9996
6	15	3	0.10	600	0.64	0.63	2.22	0.0032	0.9995
7	17	4	0.27	600	0.84	0.87	-3.46	0.0065	0.9989
8	18	4	0.27	800	0.89	0.91	-2.12	0.0042	0.9996
9	21	2	0.62	800	0.72	0.74	-3.25	0.0052	0.9990
10	22	3	0.45	600	0.96	0.96	0.50	0.0011	1.0000
11	23	2	0.27	300	0.92	0.91	1.36	0.0028	0.9998
12	24	4	0.62	200	1.09	1.04	4.59	0.0112	0.9977
13	25	2	0.80	1000	0.87	0.89	-2.29	0.0045	0.9995
14	10	3	0.62	900	0.37	0.39	-4.64	0.0038	0.9980
15	11	4	0.45	800	0.47	0.48	-1.72	0.0018	0.9997
16	12	2	0.80	300	0.39	0.38	1.57	0.0014	0.9997
17	13	3	0.80	600	0.46	0.45	2.94	0.0030	0.9991
18	14	4	0.60	700	0.64	0.63	1.88	0.0027	0.9996
19	9	2	0.27	800	0.37	0.38	-2.38	0.0020	0.9995
20	25	4	0.27	1000	1.16	1.06	8.62	0.0224	0.9911
						Average error: 3.30% *Average RMSE: 0.0048* *Average R^2: 0.998*			

where; p is the predicted value, a the actual value and n the number of samples.

4 RESULTS AND DISCUSSION

The comparisons of experimental results with the ANN predictions have been depicted in terms of percentage error for validation set of experiments. From **Table 3** it is evident that for our set of data the neural network predicts the surface roughness nearer to the experimental values. In the prediction of surface roughness values the average errors for ANN is found to be as 3.30 %.

The average *RMSE* was found to be as 0.0048. The value of the multiple coefficient of R^2 between experimental results and ANN prediction is obtained as 0.998. This value showed that ANN model fits well with

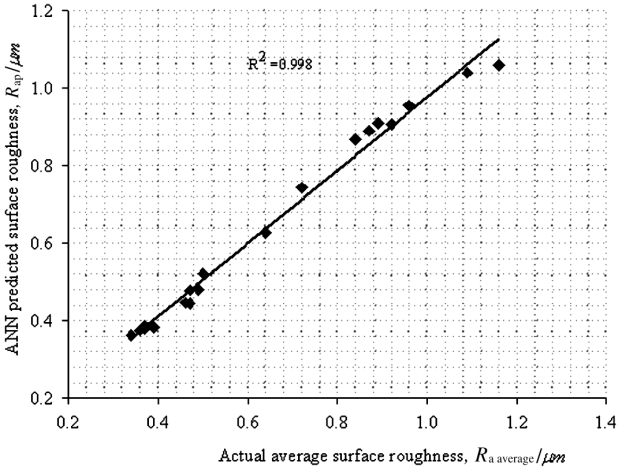

Figure 6: Actual average surface roughness against ANN prediction
Slika 6: Dejanska hrapavost proti ANN-napovedi

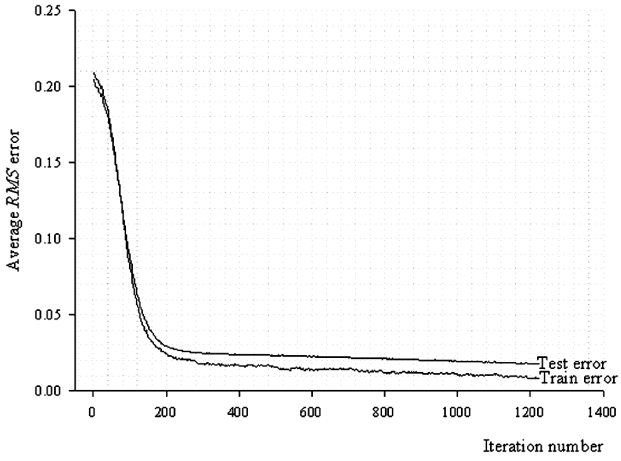

Figure 7: Learning behavior of ANN model
Slika 7: Učno vedenje ANN-modela

the experimental results. **Figure 6** illustrates the ANN predictions against the experimental results.

The training of the neural network was performed with an allowable error of 0.01 (sum of squared error over the output neurons). The learning behavior of this particular network is shown in **Figure 7**.

5 CONCLUSION

In this study, for the modeling of the effects of ball burnishing parameters (burnishing force, number of passes, feed rate and burnishing speed) on the surface roughness of the AA 7075 aluminum alloy depending on various processing parameters, an ANN-based approach has been suggested and successfully implemented. As **Figure 6** indicates for each average surface roughness value the predictions of the ANN are very close to the experimental results. It may be concluded that the ANN may be used as a good alternative for the analysis of the effects of burnishing parameters on the average surface roughness. In the field of surface roughness, ANNs are good alternative to conventional empirical modeling. The advantages of the ANN compared to classical methods are speed, simplicity and capacity to learn from the experimental results and also none need for a wider experimental study. Because of this fact that, engineering effort may be reduced in the areas where ANN modeling is preferred.

In this study the focus was to predict the average surface roughness in ball burnishing process. The results from ANN model will allow to improve determination of the average surface roughness value and help to determine in a short time the behavior of the experimental results.

6 REFERENCES

[1] P. G. Benardos, G. C. Vosniakos, Robotics and Computer Integrated Manufacturing, 18 (**2002**), 343–354

[2] C. Feng, X. Wang, In.t J. Adv. Manuf. Technol., 20 (**2002**), 1–8

[3] A. M. Hassan, Journal of Materials Processing Technology, 72 (**1997**), 385–391

[4] C. Wick, R. F. Veilleux, Tool and manufacturing engineers handbook, Soc. Manuf Eng, (**1985**), 16–38

[5] T. Siva Prasad, B. Kotiveerachari, J. Inst. Eng. India, 69 (**1998**), 55–58

[6] N. H. Loh, S.C. Tam, S. Miyazawa, Int. J. Mach. Tools Manuf., 33 (**1993**), 841–852.

[7] A. M. Hassan, A. S. AL-Bsharat, Wear, 199 (**1996**), 1–8

[8] A. M. Hassan, A. S. AL-Bsharat, J. Mater. Process. Technol., 59 (**1996**), 250–256

[9] R. L. Murthy, B. Kotiveerachari, Prec. Eng., 3 (**1981**), 172–179

[10] R. Rajasekariah, S. Vaidyanathan, Wear, 34 (**1975**), 183–188

[11] Y. G. Shneider, Mach. Tooling, 38 (**1967**), 19–22

[12] H. K. Durmus, E. Ozkaya, C. Meric, Materials and Design, 27 (**2006**), 156–159

[13] M. Perzyk, A.W. Kochanski, Journal of Materials Processing Technology, 109 (**2001**), 305–307

[14] M. Y. Rafiq, G. Bugmann, D.J. Easterbrook, Comput. Struct., 79 (**2001**), 1541–1552

[15] S. Kenig, A. B. David, O. M. Sadeh, Eng. Appl. Artif. Intel., 14 (**2001**), 819–823

[16] R. Song, Q. Zhang, M. Tseng, B. Zang, Mater. Sci. Eng., C3 (**1995**), 39–41

[17] M. Nalbant, H. Gokkaya, I. Toktas, G. Sur, Robotics and Computer Integrated Manufacturing, 2008, doi:10.1016/j.rcim.2007.11.004

[18] E. Oztemel, Integrating expert systems and neural networks for intelligent on-line statistical process control. PhD thesis, School of Electrical, Electronic and Systems Engineering, University of Wales, Cardiff, (**1992**), 1–38

[19] MATLAB 6.5, The Language of Technical Computing release 13, Natick, The MathWorks, Inc., (2002)

[20] E. Arcaklýoglu, I. J. Energy Res., 28 (**2004**), 1113–1125

[21] A. Sozen, E. Arcaklýoglu, M. Ozalp, N. Caglar, Renewable Energy, 30 (**2005**), 1075–1090

[22] A. Sozen, E. Arcaklýoglu, M. Ozkaymak: Appl. Energy, 81 (**2005**), 209–210

[23] I. Toktas, N. Akturk, A new approach using artificial neural Networks for conceptual design of cylindrical helical gears. In Proceedings of the MTET 2005 1st international vocational and technical education technologies congress, Marmara University, Istanbul/ Turkey, (**2005**), 754–762

UDK 620.178.1:666.3/.7
Strokovni članek/Professional article

ISSN 1580-2949
MTAEC9, 42(5)221(2008)

MERJENJE OBRABNE OBSTOJNOSTI STRUKTURNE KERAMIKE Al_2O_3

WEAR-RESISTANCE MEASUREMENT OF STRUCTURAL Al_2O_3 CERAMICS

[1]Milan Ambrožič, [2]Stojana Veskovič Bukudur, [1]Tomaž Kosmač, [1]Kristoffer Krnel, [1]Darko Eterovič, [1]Natalija Petkovič Habe, [1]Irena Pribošič

[1]Odsek za inženirsko keramiko (K6), Institut "Jožef Stefan", Jamova 39, Ljubljana, Slovenija
[2]Hidria AET, d. o. o., Poljubinj 89, Tolmin, Slovenija

Prejem rokopisa – received: 2008-02-15; sprejem za objavo – accepted for publication: 2008-03-31

Obstojnost keramike proti obrabi med vsakdanjo uporabo je poleg drugih mehanskih lastnosti – trdote, togosti, tlačne in natezne trdnosti ter žilavosti – velikega pomena. Pri obrabni obstojnosti so pomembne mnoge lastnosti, kot so trdota, žilavost, koeficient trenja med stičnimi površinami, morebitne kemične reakcije zaradi močno povišane temperature in nastanek »triboplasti«, tako da je zelo težko najti enolično povezavo med danimi veličinami. Zato je treba obrabno obstojnost posebej kvantitativno opredeliti in jo izmeriti v ponovljivih razmerah. V članku opisujemo preprost in poceni način merjenja obrabne obstojnosti strukturne korundne keramike z običajno napravo za brušenje in poliranje keramičnih vzorcev.

Ključne besede: strukturna keramika, obrabna obstojnost, faktor obrabe

Wear resistance of ceramics in the every-day use is of great importance, besides other mechanical properties, e.g., hardness, stiffness, compressive and tensile strength and toughness. Several characteristics contribute to wear resistance, such as hardness, toughness, coefficient of friction between the surfaces in contact, possible chemical reactions due to highly increased temperature, and the formation of tribofilm, making the search for the unique connection between these quantities very difficult. Therefore, it is necessary to define the wear resistance quantitatively and measure it in repeatable circumstances. A simple and cost-efficient method for wear-resistance measurement of the structural ceramic material alumina with the help of the ordinary grinding/polishing machine for ceramic samples is presented.

Key words: structural ceramics, wear-resistance, wear factor

1 UVOD

Pomembni področji uporabe strukturne keramike sta inženirska in protetična keramika. Strukturna keramika mora imeti zadovoljive mehanske lastnosti: veliko trdnost in trdoto ter čim boljšo žilavost. Kjer pa je njena površina izpostavljena vsakodnevnemu trenju z drugimi stičnimi površinami, npr. v sklepnih keramičnih protezah, mora imeti tudi dobro obstojnost proti obrabi.

Zato je treba obrabno obstojnost kvantitativno opredeliti in jo meriti v čim bolj ponovljivih razmerah. Osnova sodobnih meritev na komercialnih napravah je preprosta: z določeno silo je treba pritisniti površino merjenca ob referenčno površino (referenčna površina je lahko iz enakega ali pa drugačnega materiala kot preskušani vzorec), spraviti drsni površini v relativno gibanje in nazadnje izmeriti učinke obrabnega preskusa, npr. izmeriti zmanjšanje prostornine merjenca. Veliko obrabnih preskusov je bilo narejenih na dveh pomembnih inženirskih in biomedicinskih keramičnih materialih: aluminijevem in cirkonijevem oksidu (Al_2O_3 in ZrO_2) in njunih kompozitov.[1-11] Aluminijev oksid (Al_2O_3) – korundna keramika – ima veliko trdoto in zato tudi veliko obrabno obstojnost. Danes se veliko uporablja merilo, da je material dobro obrabno obstojen v vsakdanji uporabi, če ima faktor obrabe po enačbi (1) manjši od vrednosti 10^{-6} mm^3/J.[8,10]

Za vedenje trdih materialov pri trenju in obrabi se je uveljavilo tudi ime "tribološke lastnosti materialov". Ime izhaja iz tega, ker pri stiku in relativnem gibanju razmeroma gladkih površin dveh trdih materialov nastane med njima še tretja plast, na kratko triboplast, in sicer iz aglomeriranih odkrušenih delčkov z ene ali obeh keramičnih površin.[6] Kemijsko in fazno sestavo triboplasti ter njeno hrapavost, ki seveda močno vpliva na koeficient trenja, lahko preučimo z vrstičnim in presevnim elektronskim mikroskopom (SEM in TEM), rentgensko spektroskopijo, mikroskopom na atomsko silo (AFM), ramansko spektroskopijo, optičnim mikroskopom – profilometrom itd.[1-10] Več poskusov kaže na to, da se po začetnem spreminjanju koeficient trenja med stičnima površinama ustali pri neki vrednosti, kar kaže na to, da ga zares določa nastala triboplast.[6,7,11]

Krell in Klaffke sta primerjala obrabo površin vzorcev Al_2O_3, tetragonalnega ZrO_2 (z molskim deležem Y_2O_3 3 %) in kompozita Al_2O_3/TiC (TiC je titanov karbid) pri drgnenju ob krogle iz Al_2O_3 pri različnih pogojih (npr. različni vlažnosti zraka).[3] Pri tem je imela keramika Al_2O_3 različne povprečne velikosti zrn, od 0,4 μm do 3 μm, odvisno od majhne količine dodatkov, npr. MgO, ki imajo bistven vpliv na potek sintranja. Za Al_2O_3 sta ugotovila, da se z zmanjšanjem kristalnih zrn zmanjša faktor obrabe. Nadalje, vlažen zrak ali tekoča voda med stičnima površinama zmanjšata koeficient

trenja, kar v glavnem vodi do zmanjšanja faktorja obrabe. Faktorja obrabe Al_2O_3 in kompozita Al_2O_3/TiC sta podobna, obraba ZrO_2 pa je večja.

Liu in sodelavci so ugotovili, da dodatek 6 % (prostorninski delež) diopsida, $MgCa(SiO_3)_2$ precej izboljša tribološke lastnosti keramike Al_2O_3.[10] Med drugim so potrdili splošno znano dejstvo, da pri večjih normalnih silah med drsnimi površinami nastane bolj izrazito puljenje celih zrn, s čimer se močno poveča obraba. Njihova najpomembnejša ugotovitev pa je verjetno ta, da se faktor obrabe $k = 10^{-6}$ mm^3/J za čisti Al_2O_3 pri danih pogojih preskusa zmanjša na desetino vrednosti pri 12-odstotnem deležu diopsida.

Čeprav obstajajo komercialne naprave za merjenje obrabne obstojnosti materialov na osnovi enačbe (1), pa si lahko pomagamo tudi z improviziranimi preskusi na običajni napravi za brušenje in poliranje keramičnih vzorcev. Na tak način smo na Odseku za inženirsko keramiko Instituta "Jožef Stefan" izmerili obrabno obstojnost keramike Al_2O_3, pripravljene na različne načine in z različnimi primesmi.

2 OPREDELITEV OBRABNE OBSOJNOSTI KERAMIKE

Obraba materiala pri drgnenju ob enak ali drugačen material je tem večja, čim večja je sila trenja med površinama, ta sila pa narašča s pravokotno silo, ki tišči podlagi eno ob drugo. Obraba narašča tudi s časom drgnjenja oziroma z relativnim premikom med stičnima površinama. Zato je smiselno opredeliti faktor obrabe k takole:

$$k = \frac{\Delta V}{F_n s} \qquad (1)$$

kjer je ΔV zmanjšanje volumna materiala oz. preskusnega vzorca zaradi obrabe, F_n je pravokotna (normalna) sila med stičnima površinama, s pa je razdalja, ki jo pri trenju naredi ena površina relativno glede na drugo. Primerna enota za faktor obrabe je npr. mm^3/J. Enačba (1) je v skladu s pričakovanjem, da je zmanjšanje volumna materiala sorazmerno z delom zunanje sile, saj je za trganje medatomskih vezi v materialu potrebna energija, število potrganih vezi pa je sorazmerno tako z volumnom odnesenega materiala kot z dovedeno notranjo energijo. Zavedati pa se moramo, da ta sorazmernost velja le do določene mere, saj so prisotni različni mehanizmi odnašanja materiala s površine. Po drugi strani je sila trenja F_{tr} med stičnima povšinama bolj vplivna od normalne sile F_n, saj je delo sile trenja, ki je vzporedna z relativnim gibanjem obeh površin, različno od nič, medtem ko je delo normalne sile nič. Sila trenja je sicer sorazmerna z normalno silo, vendar pa je odvisna tudi od koeficienta trenja k_{tr}: $F_{tr} = k_{tr}F_n$. Tako je lahko pri isti normalni sili F_n in pri sicer enaki keramiki hitrost obrabe zelo različna, če imamo različne koeficiente trenja med stičnima površinama, npr. zaradi oblivanja površin z vodo. Vendar, če je pri neki aplikaciji koeficient trenja vedno enak, je normalna sila sorazmerna s silo trenja, tako da je enačba (1) smiselna.

3 EKSPERIMENTALNO DELO

Zaradi sodelovanja z industrijo (AET – Hidria, Tolmin) nas je zanimala obrabna obstojnost aluminijevega oksida Al_2O_3. Obrabne preskuse lahko naredimo kar na napravi za poliranje keramičnih vzorcev, če poskrbimo za ponovljive pogoje preskušanja. Postopek obrabnih preskusov na okroglih ploščicah (tabletkah) z uporabo diamantne paste z delci povprečne velikosti 45

Slika 1: a) Struersova polirna naprava z nastavkom Pedepin 2; b) Povečan izrez naprave z nosilcem vzorcev in vpetim preskusnim vzorcem
Figure 1: a) Struers polishing machine with the part Pedepin 2; b) Enlarged section of the machine with the sample holder and attached testing sample

Tabela 1: Vrsta in mere vzorcev: ρ = gostota, M = masa, D_{zun} in D_{not} = zunanji in notranji premer, L = dolžina
Table 1: Type and dimensions of the samples: ρ = density, M = mass, D_{zun} and D_{not} = outer and inner radius, respectively, L = length

Skupina	Tip	ρ/(g/cm^3)	M/g	D_{zun}/mm	D_{not}/mm	L/mm
1	MR52-23	3,76	20,66	9,95	2,30	77,07
2	MR32-23	3,76	20,78	9,95	2,30	77,13
3	KMS96	3,77	21,45	10,21	2,10	77,17
4	Alcoa	3,92	21,52	9,95	2,30	77,22
5	Rjava	3,92	24,08	9,95	2,77	89,13
6	AET	3,78	22,60	10,53	2,30	76,8

μm je bil podrobneje opisan v reviji Vakuumist.[12] Tu opišemo obrabne preskuse, kjer smo vzorce brusili na napravi Pedepin 2 danskega podjetja Struers (**slika 1a**). Iz podjetja AET smo prejeli vzorce v obliki votlih valjev z merami v **tabeli 1**. Vzorci so gredi vodnih črpalk iz serijske proizvodnje. Od celotne dolžine vzorcev smo za posamezni preskus odrezali kose, dolge okrog 20 mm (**slika 1b**). Keramik je bilo šest vrst, glede na vrsto uporabljenih keramičnih prahov in dodanih primesi. Na primer oznaka AET (tip 6) pomeni keramiko iz mešanice več vrst začetnih prahov, ki jih v AET navadno uporabljajo za serijsko proizvodnjo bele korundne keramike, medtem ko ima rjava keramika (tip 5) primešan manganov in titanov oksid. Značilna temperatura sintranja teh vzorcev je bila 1640 °C, le za rjavo keramiko je bila ta temperatura 1300 °C. Gostote keramik so bile izmerjene z Arhimedovo metodo, čeprav bi jih lahko preprosto izračunali iz mase in dimenzij vzorcev.

Že pri žaganju preskusnih dvocentimetrskih kosov z diamantno žago pri ponovljivih pogojih (enaka obtežba, temeljito očiščenje lista žage pred žaganjem itd.) smo dobili prvo dokaj zanesljivo informacijo o obrabni obstojnosti različnih keramik. Časi žaganja, ki so se gibali okrog vrednosti 5 min ali več, so se namreč za različne skupine zelo razlikovali, medtem ko so si bili za vzorce iz iste keramike med seboj podobni. Daljši čas žaganja nakazuje večjo obrabno obstojnost keramike (**tabela 2**). Sam obrabni preskus na napravi Pedepin je potekal takole: Vzorec smo pritrdili na natančno označeno mesto na nosilcu in ga najprej na kratko zbrusili z bolj grobo brusno ploščico z diamantnimi zrni, tako da smo poskrbeli za planparalelnost obdelovalne površine z drugo brusno ploščico v nadaljevanju preskusa. Vzorec smo stehtali, nato pa ga obrusili s finejšo ploščico trikrat po 1 min (za preskus ponovljivosti). Po vsaki minuti brušenja s finejšo ploščico smo vzorec ponovno stehtali in izračunali izgubo mase/volumna. Pred vsakim tehtanjem smo vzorec očistili v ultrazvočni kopeli z acetonom. Zelo pomembno za ponovljivost rezultatov je bilo tudi čiščenje brusnih ploščic pred vsakim preskusom.

4 REZULTATI IN DISKUSIJA

Ker smo preskuse izvajali pri nespremenljivih pogojih (stalna normalna sila $F_n \approx 50$ N, frekvenca vrtenja brusne ploščice 917 min^{-1}, frekvenca vrtenja nosilca vzorcev 300 min^{-1} itd.), nismo vsakič računali faktorja obrabe po enačbi (1), temveč nam je zadostovala primerjava zmanjšanja njihove prostornine. Izidi meritev so prikazani v **tabeli 2**. Naprava Pedepin nima vgrajenega merilnika normalne sile, zato je zgoraj omenjena vrednost 50 N le groba ocena, ki smo jo dobili z uporabo tehtnice. Na osnovi podatkov iz tabele ($<V> \approx 100$ mm^3), ocenjene sile ($F_n \approx 50$ N) in relativne drsne poti ($s \approx 65$ m, izračunali smo jo na osnovi frekvenc vrtenja (števila obratov na minuto) polirne ploščice in nosilca vzorca, ekscentričnosti osi obeh vrtenj in časa preskusa) smo ocenili faktor obrabe: $k \approx 0{,}03$ mm^3/J. Ta vrednost je zelo velika v primerjavi s tistimi, navedenimi pri običajnih preskusnih pogojih v literaturi, vendar pa je brušenje z brusno ploščico veliko bolj agresivno kot npr. medsebojno drgnjenje gladkih keramičnih površin. Žaganih površin vzorcev nismo spolirali pred preskusom z brušenjem in pričakovati je bilo, da bi bila obraba na začetku spoliranih površin veliko manjša. Dodatni preskusi so pokazali, da zmanjšanje volumna vzorcev ni premo sorazmerno s časom, temveč se hitrost obrabe zaradi nastanka triboplasti hitro zmanjšuje. Za primerjavo: faktor obrabe za laboratorijske Al_2O_3-tabletke, na katerih smo naredili predhodne obrabne preskuse z drgnjenjem ob fino polirno ploščo, na katero smo polivali redko vodno suspenzijo diamantnih delcev povprečnega premera 45 μm,[12] je bil $6 \cdot 10^{-4}$ mm^3/J, vrstni red različnih keramik po obrabni obstojnosti pa je bil podoben kot pri preskusu z brusno ploščico. Ena najpomembnejših veličin pri obrabi materiala, koeficient trenja, namreč zelo variira pri različnih preskusnih pogojih. Kljub tem razlikam pa je preskus z diamantno brusno ploščico poceni, preprost in hiter, daje osnovno informacijo o obrabni obstojnosti in tudi obdelovalnosti različnih keramik, obe lastnosti (oziroma kompromis med njima) pa sta pomembni za industrijsko tehnologijo.

Časa žaganja pri vzorcih skupin 3 in 6 sta samo informativna, saj imajo ti vzorci bistveno drugačno ploščino prereza (**tabela 1**), čas žaganja pa je seveda odvisen tudi od te veličine. Po drugi strani smo ugotovili, da različni prerezi vzorcev skoraj nič ne vplivajo na zmanjšanje volumna med preskusom; to smo preverili s primerjavo zmanjšanja volumna za isto keramiko (isti votli valj na njegovem koncu, ki ima drugačen premer votline kot v sredini valja). Iz tabele 2 je razvidno, da imajo keramike skupin 2, 3 in 6 približno

enako obrabno obstojnost, sledi keramika 1, manj obstojni pa sta keramiki 4 in 5. Časi žaganja potrjujejo rezultate za zmanjšanje volumna med preskusi: večji volumenski obrabi ustreza daljši čas žaganja vzorcev.

Tabela 2 Rezultati žaganja in obrabnega preskusa: <*t*> in δ*t* sta povprečni čas in standardna deviacija časa žaganja vzorcev z diamantno žago (3 ali 4 meritve), <*V*> in δ*V* sta povprečno zmanjšanje volumna vzorcev med enominutnim preskusom in ustrezna standardna deviacija (3 meritve)

Table 2 Results of sawing and wear test: <*t*> and δ*t* are average time of sawing of samples with the diamond saw and its standard deviation, respectively (3 or 4 measurements), <*V*> and δ*V* are average volume loss of samples after 1-minute test and the corresponding standard deviation, respectively (3 measurements)

Skupina	<*t*>/(min:s)	δ_t /s	<*V*>/mm^3	δV/mm^3
1	6:44	7	106	6
2	7:28	7	79	2
3	6:26 (inf)	–	78	3
4	5:11	12	147	10
5	4:08	4	158	1
6	8:09 (inf)	–	83	1

Površine vzorcev po žaganju in preskusnem brušenju smo si ogledali z vrstičnim elektronskim mikroskopom (SEM). **Slika 2** prikazuje značilno površino po žaganju in brušenju. Slike za vse vrste keramike so si podobne. S slike lahko razberemo, da je glavni mehanizem pri žaganju in brušenju abrazija kristalnih zrn z diamantnimi delci, puljenje celih kristalnih zrn s površine pa je manj pomembno.

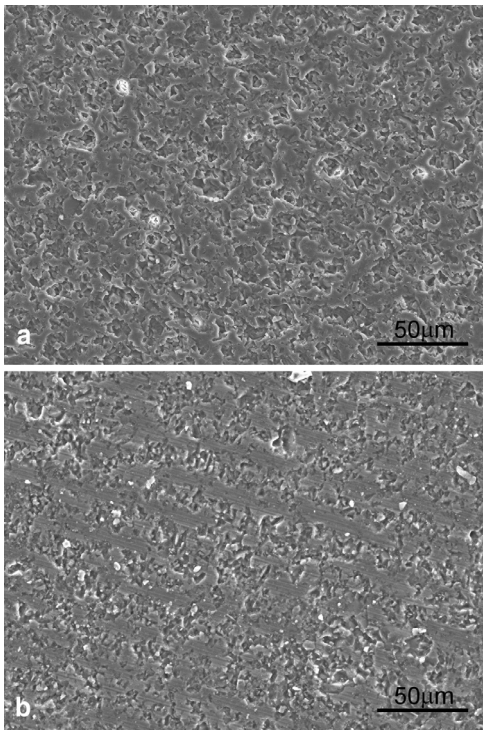

Slika 2: SEM-fotografija žagane (a) in brušene (b) površine keramike skupine 3

Figure 2: SEM-photograph of the sawed (a) and ground (b) surface of the ceramics from group 3

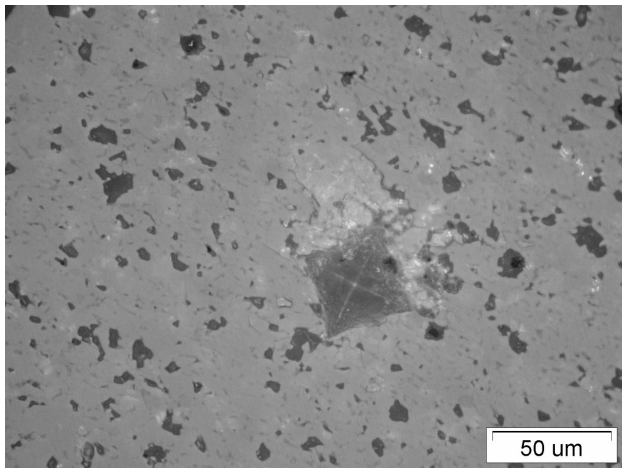

Slika 3: Fotografija slike optičnega mikroskopa površine keramike skupine 3 z odtisom Vickersove piramide. Na sliki je dobro opazna tudi poroznost keramike.

Figure 3: Optical-microscope photograph of the surface of ceramics from group 3 with the Vickers-pyramid indentation. The porosity of the ceramic material is also evident.

Izmerili smo tudi trdoto različnih keramik z Vickersovim odtisom z diamantno piramido pri dveh obtežitvah, 2 kg in 5 kg. Pri tej metodi izračunamo trdoto z velikostjo odtisa (pod optičnim mikroskopom vidimo kvadrat, **slika 3**, sicer pa ima odtis obliko pravilne 4-strane piramide). Značilne vrednosti trdote so okrog 15 GPa, med različnimi keramikami so sicer vidne razlike v trdoti, a precej manjše kot razlike v obrabnem preskusu in tudi ni očitne korelacije med trdoto in obrabno obstojnostjo. Na slikah z optičnega mikroskopa smo ocenili poroznost keramik: le-ta je velikostnega reda 10 % in ni opaziti bistvenih razlik za različne keramike. Enako velja za povprečno velikost in velikostno porazdelitev por: pore so v povprečju velike nekaj mikrometrov in so pri rjavi keramiki nekaj manjše kot drugod. Povprečno velikost kristalnih zrn smo izračunali z analizo SEM (Scanning Electron Microscope = vrstični elektronski mikroskop)-slik poliranih in termično jedkanih površin keramičnih vzorcev, njena vrednost pa je okrog 3 μm. Različne keramike torej nimajo očitnih razlik v mikrostrukturi in je verjetno za njihovo različno obrabno obstojnost odločilna morebitna razlika v strukturi snovi med kristalnimi zrni.

5 SKLEP

Tudi z improviziranimi preprostimi preskusi na standardni napravi za brušenje in poliranje vzorcev se da dokaj zanesljivo primerjati obrabno obstojnost različnih keramičnih materialov.

6 LITERATURA

[1] Birkby I., Harrison P., Stevens R., The effect of surface transformation on the wear behaviour of zirconia TZP ceramics, J. Eur. Ceram. Soc. 5 (**1989**), 37–45

[2] Fischer T., Anderson M. P., Jahanmir S., Influence of fracture toughness on the wear resistance of yttria-doped zirconium oxide, J. Am. Ceram. Soc. 72 (**1989**) 2, 252–257

[3] Krell and D. Klaffke, Effects of grain size and humidity on fretting wear in fine-grained alumina, Al_2O_3/TiC, and zirconia, J. Am. Ceram. Soc. 79 (**1996**) 5, 1139–1146

[4] Gee M. G., Jennett N. M., High resolution characterisation of tribochemical films on alumina, Wear 193 (**1996**) 2, 133–145

[5] Morita Y., Nakata K., Ikeuchi K., Wear properties of zirconia/alumina combination for joint prostheses, Wear 254 (**2003**) 1–2, 147–153

[6] Kalin M., Hockey B., Jahanmir S., Wear of hydroxiapatite sliding against glass-infiltrated alumina, J. Mater. Res. 18 (**2003**) 1, 27–36

[7] Basu B., Vleugels J., Van der Biest O., Microstructure-toughness-wear relationship of tetragonal zirconia ceramics, J. Eur. Ceram. Soc. 24 (**2004**) 7, 2031–2040

[8] Kerkwijk B., Garcya M., Van Zyl W. E. et al., Friction behaviour of solid oxide lubricants as second phase in α–Al_2O_3 and stabilised ZrO_2 composites, Wear 256 (**2004**), 182–189

[9] Novak S., Kalin M., Lukas P., Anne G., Vleugels J., Van der Biest O., The effect of residual stresses in functionally graded alumina-ZTA composites on their wear and friction behaviour, J. Eur. Ceram. Soc. 27 (**2007**) 1, 151–156

[10] Liu C., Zhang J., Sun J., Zhang X., Tribological properties of pressureless sintered alumina matrix ceramic materials improved by diopside, J. Eur. Ceram. Soc., in print

[11] Singha Roy R., Guchhait H., Chanda A., Basu D., Mitra M. K., Improved sliding wear-resistance of alumina with sub-micron grain size: A comparison with coarser grained material, J. Eur. Ceram. Soc., 27 (**2007**), 4737–4743

[12] Ambrožič M., Obrabna obstojnost keramike, Vakuumist 27 (**2007**) 3, 10-15

DOKTORSKA, MAGISTRSKA IN DIPLOMSKA DELA – DOCTOR'S, MASTER'S AND DIPLOMA DEGREES

DOKTORSKA DELA – DOCTOR'S DEGREES

Na Naravoslovnotehniški fakulteti Univerze v Ljubljani je dne 7.7.2008 pred komisijo v sestavi: red. prof. dr. Radomir Turk kot predsednik in člani: red. prof. dr. Ladislav Kosec, red. prof. dr. Anton Smolej in izr. prof. dr. Tomaž Rodič **Aleš Nagode**, univ. dipl. inž. materialov in metalurgije zagovarjal doktorsko disertacijo z naslovom:

Analiza lezenja jekla 9Cr-1Mo-0,2V z upoštevanjem napetostno odvisne aktivacijske energije
An analysis of the creep behaviour of 9Cr-1Mo-0.2V steel based on the stress-dependent activation energy

Doktorska disertacija je izdelana pod mentorstvom red. prof. dr. Ladislava Kosca.

ANALIZA LEZENJA JEKLA 9Cr-1Mo-0,2V Z UPOŠTEVANJEM NAPETOSTNO ODVISNE AKTIVACIJSKE ENERGIJE

UDK: 539.3:669.14.018

POVZETEK

Vedenja jekla 9Cr-1Mo-0,2V pri kratkotrajnih preizkusih lezenja ni mogoče opisati z navadnim potenčnim zakonom Arrheniusovega tipa, saj je izmerjen napetostni eksponent n, definiran kot $(\partial \ln \dot{\varepsilon}_{min}/\partial \ln \sigma)_T$, zelo odvisen od temperature, izmerjena navidezna aktivacijska energija lezenja Q_c, definirana kot $(\partial \ln \dot{\varepsilon}_{min}/\partial(-1/RT))_\sigma$, pa od napetosti.

Problema opisa vedenja tega jekla pri lezenju smo se najprej lotili z uporabo koncepta napetostnega praga (*threshold stress*), to je z uvedbo mejne napetosti, pod katero je lezenje zanemarljivo. Izpeljali smo enačbo, ki sicer dobro opiše vedenje jekla pri lezenju, vendar pa se je izkazalo, da je mejna napetost σ_{th} močno odvisna od temperature in/ali uporabljene napetosti ter celo spreminja predznak. Nizka vrednost izračunane navidezne aktivacijske energije lezenja, ki je dosegla le 185 kJ mol^{-1}, kar je celo manj od aktivacijske energije za samodifuzijo v Fe-α, pa je v tem primeru irelevantna za pojasnjevanje delujočih mehanizmov lezenja.

Za opis vedenja jekla 9Cr-1Mo-0,2V pri lezenju smo zato teoretično razvili nov model potenčnega zakona lezenja z napetostno odvisno energijsko pregrado. Glede na standardni model temelji naš na hipotezi, po kateri delujoča napetost neposredno vpliva tudi na aktivacijsko

AN ANALYSIS OF THE CREEP BEHAVIOUR OF 9Cr-1Mo-0.2V STEEL BASED ON THE STRESS-DEPENDENT ACTIVATION ENERGY

UDC: 539.3:669.14.018

ABSTRACT

The creep behaviour of 9Cr-1Mo-0.2V steel during short-term creep tests cannot be accurately described by a simple Arrhenius-type power-law model because the apparent stress exponent n, defined as $(\partial \ln \dot{\varepsilon}_{min}/\partial \ln \sigma)_T$, shows a strong temperature dependence, whereas the apparent activation energy of the creep Q_c, defined as $(\partial \ln \dot{\varepsilon}_{min}/\partial(-1/RT))_\sigma$, shows a strong stress dependence.

The problem of describing the creep behaviour of the examined steel was first dealt with by applying the threshold-stress concept, i.e., the introduction of the threshold stress σ_{th}, below which the creep deformation is assumed to be negligible. An equation that satisfactorily describes the creep behaviour of the examined steel was derived. However, it was observed that the threshold stress σ_{th} strongly depends on the temperature and/or the applied stress, and that sometimes it can even change its sign. The low value of the calculated activation energy of the creep, which was only 185 kJ mol^{-1}, is considerably smaller than the activation energy for self-diffusion in Fe-α, and thus it is irrelevant for an explanation of the acting creep mechanism.

For this reason, a power-law, stress-dependent energy-barrier model was theoretically developed in order to describe the creep behaviour of 9Cr-1Mo-0.2V

energijo oziroma na energijsko pregrado, ki jo je treba pri aktiviranju mehanizmov premagati, in ne samo na potencialno energijo začetnega in končnega stanja mikrostrukturnih območij, v katerih se lezenje odvija. Nov model potenčnega zakona smo izboljšali še z upoštevanjem linearne odvisnosti aktivacijskega volumna od temperature ter z normiranjem napetosti z uvedbo strižnega modula. Prvič smo ta model v še ne povsem končni obliki uspešno uporabili za opis lezenja jekla 9Cr-1Mo-0,2V na osnovi literaturnih podatkov, nato pa še za opis vedenja tega jekla pri kratkotrajnem lezenju (*ang. short term creep test*) v tem delu, pri čemer smo primerjali različne vrste preizkušancev oz. obremenitve.

Jeklo 9Cr-1Mo-0,2V smo toplotno obdelali po standardni toplotni obdelavi, nato pa opravili enoosne statično natezne preizkuse lezenja pri konstantni obremenitvi oz. konstantni napetosti ter merili lezenje še z upogibanjem tankih diskov s centralno delujočo obremenitvijo (*ang. small-punch test*), ki v preizkušancu povzroči večosno rotacijsko simetrično ter izrazito heterogeno napetostno in deformacijsko stanje. Pri enoosnih nateznih preizkusih lezenja so bile temperature lezenja 625 °C, 650 °C oz. 675 °C, napetosti pa od 120 MPa do 240 MPa, medtem ko so bile temperature preizkušanja pri merjenju lezenja z upogibanjem tankega diska 650 °C, 675 °C oz. 690 °C, obremenitve pa od 350 N do 550 N. Preizkusi merjenja lezenja z upogibanjem tankega diska so bili opravljeni na diskih različnih debelin, in sicer 0,44 mm, 0,47 mm oz. 0,50 mm.

Ugotovili smo zelo dobro ujemanje med eksperimentalnimi podatki in izračunanimi vrednostmi po modelu potenčnega zakona z napetostno odvisno energijsko pregrado. Navidezna aktivacijska energija za lezenje postane v našem modelu le še nekoliko odvisna od napetosti. Pri enoosnih statično nateznih preizkusih lezenja se s povečanjem napetosti od 120 MPa do 240 MPa napetostno odvisna navidezna aktivacijska energija lezenja Q_c, izračunana iz minimalne hitrosti lezenja $\dot{\varepsilon}_{min}$ znižuje od približno 645 kJ mol^{-1} do 600 kJ mol^{-1}, izračunana iz časa do porušitve t_r pa od približno 580 kJ mol^{-1} do 548 kJ mol^{-1}. Napetostni eksponent n pa je v obeh primerih enak, n = 4,5.

Pri merjenju lezenja z upogibanjem tankega diska je bila eksperimentalno potrjena veljavnost Monkman-Grantove odvisnosti med minimalno hitrostjo upogibanja diskov $\dot{\delta}_{min}$ in časom do porušitve $t_{r,SP}$. Zato smo lahko v izboljšanem modelu potenčnega zakona z napetostno odvisno energijsko pregrado minimalno hitrost upogibanja diska $\dot{\delta}_{min}$ ustrezno zamenjali s časom do porušitve $t_{r,SP}$, saj sta obe količini skoraj obratno sorazmerni. Ugotovili smo, da je optimalna debelina diska odvisna od geometrije naprave za merjenje lezenja in je v našem primeru med 0,48 mm in 0,50 mm. Izračunana navidezna aktivacijska energija lezenja Q_c je nekoliko odvisna od obremenitve in je za debelino diska 0,50 mm pri obremenitvi 550 N enaka 543 kJ mol^{-1}, pri obremenitvi

steel. In contrast to the standard model, this model was based on the hypothesis that the application of stress also affects the activation energy, i.e., the energy barrier that needs to be overcome when a local region transforms, and not just the potential energy of the initial and final local states. The new power-law model was additionally improved by applying the linearity between the activation volume and temperature as well as by normalising the applied stress with the shear modulus. This model was then used in a not-completely-final version for the first time to describe the already published creep data of 9Cr-1Mo-0.2V steel and then also for a description of the short-creep data in the present work, where different types of test specimens and loadings were compared.

The 9Cr-1Mo-0.2V steel underwent a standard heat treatment. After this uniaxial static-tensile creep tests at a constant load and a constant stress were conducted as well as small-punch creep tests, which led to a multiaxial, rotary-symmetric, heterogeneous stress and deformation state in the sample. While the uniaxial tensile creep tests were performed at temperatures of 625 °C, 650 °C and 675 °C and initial stresses ranging from 120 MPa to 240 MPa, the small-punch tests were performed at temperatures of 650 °C, 675 °C and 690 °C and at loads ranging from 350 N to 550 N. In the case of the small punch the creep properties were measured on disks with different thickness, i.e., 0.44 mm, 0.47 mm and 0.50 mm.

A very good correlation between the power-law, stress-dependent energy-barrier model and the experimental data was obtained. However, the apparent activation energy shows less stress dependence than when using the Arrhenius-type power-law. During uniaxial static-tensile creep tests the stress-dependent activation energy Q_c calculated from the minimum creep rate $\dot{\varepsilon}_{min}$ decreased from approximately 645 kJ mol^{-1} to 600 kJ mol^{-1} as the stress increased from 120 MPa to 240 MPa, while the stress-dependent activation energy calculated from the time-to-rupture t_r decreased from approximately 580 kJ mol^{-1} to 548 kJ mol^{-1}. The stress exponent n was the same in both cases, i.e., n = 4.5.

The validity of the Monkman-Grant relationship between the minimum deflection rate $\dot{\delta}_{min}$ and the time-to-rupture $t_{r,SP}$ for the small-punch creep test was experimentally confirmed. Thus, the minimum deflection rate $\dot{\delta}_{min}$ in the improved power-law, stress-dependent energy barrier model was replaced by the time-to-rupture $t_{r,SP}$, since both parameters are almost inversely proportional. It was found that the optimum disk thickness is dependent on the geometry of the small-punch apparatus for measuring the creep properties. In our case the optimum disk thickness was found to be between 0.48 mm and 0.50 mm. The calculated apparent activation energy of the creep Q_c was slightly load dependent. The value of the apparent activation energy for a disk thickness of 0.50 mm was

350 N pa 533 kJ mol^{-1}. Vrednost obremenitvenega eksponenta n_{SP} pa je pri vseh debelinah diska 4,5, kar je enako kot pri standardnih enoosnih nateznih preizkusih lezenja.

543 kJ mol^{-1} at a load of 550 N, and 533 kJ mol^{-1} at a load of 350 N. The value of the stress exponent n_{SP} was 4.5 for all the disk thicknesses and was the same as during the conventional uniaxial tensile creep tests.

Na Fakulteti za elektrotehniko Univerze v Ljubljani je dne, 2.7.2008, pred komisijo v sestavi prof. dr. Stanislav Kovačič in člani prof. dr. Drago Matko, prof. dr. Borut Zupančič in izr. prof. dr. Tomaž Kolenko **Franci Vode**, univ. dipl. inž. zagovarjal doktorsko disertacijo z naslovom:

Razvoj sistema vodenja kontinuiranih peči za ogrevanje vložka po predpisanih krivuljah ogrevanja
Development of continuous furnace control system for stock reheating according to the prescribed reheating curves

Doktorska disertacija je izdelana pod mentorstvom red. prof. dr. Draga Matka.

RAZVOJ SISTEMA VODENJA KONTINUIRANIH PEČI ZA OGREVANJE VLOŽKA PO PREDPISANIH KRIVULJAH OGREVANJA

UDK: 621.771:519.68

POVZETEK

V disertaciji je predstavljen splošen koncept kontroliranega ogrevanja vložka v kontinuirnih pečeh v jeklarski industriji, predstavljen na primeru potisne peči v podjetju ACRONI, d. o. o. Vodenje ogrevanja slabov je izvedeno z regulacijskim sledenjem referenčni krivulji ogrevanja (RKO) vsakega posameznega slaba, pri čemer regulacija temelji na matematičnem modelu ogrevanja slabov, ki deluje v realnem času. RKO je podana kot funkcija časa. Časovno podan potek RKO omogoča elegantno in natančno obravnavo zastojev. Sistem vodenja kot odziv na zastoj v proizvodnji premakne časovno definirano RKO za čas trajanja zastoja. S tem je omogočeno zaprtozančno vodenje ogrevanja slabov tudi med zastoji, in sicer še vedno po RKO. Od učinkovite in natančne obravnave zastojev je najbolj odvisna učinkovitost ter energetski prihranki na peči pri uporabi razvitega sistema. Zastoje zato sistematično razdelimo v pet različnih vrst. Najprej jih ločimo na tiste, katerih trajanja ne poznamo, in na tiste, katerih trajanje poznamo. Zadnje delimo na predvidene, nepredvidene, na zastoje zaradi različnih časov ogrevanja različnih jekel oz. debelin jekel ter na zastoje zaradi sinhronizacije z valjarskimi ogrodji. Slednji omogočajo upoštevanje kapacitet valjarskih prog pri načinu ogrevanja v peči. Za vsako vrsto zastoja določimo časovno premaknitev RKO in podaljšanje intervala pomika slabov. RKO so ločeno definirane za različne začetne temperature s korakom 50 °C. Za potrebe prehoda iz ročnega v avtomatsko vodenje so začetne RKO posnetek stacionarnega poteka ogrevanja, kakršnega predpisujejo tehnološka navodila o ogrevanju. S tem se izognemo spremembi načina ogrevanja ob uvajanju sistema v proizvodnjo. RKO je možno kadarkoli optimizirati in spremembe vnesti v tabelo RKO v podatkovni zbirki. Na koncu dela je

DEVELOPMENT OF CONTINUOUS FURNACE CONTROL SYSTEM FOR STOCK REHEATING ACCORDING TO THE PRESCRIBED REHEATING CURVES

UDC: 621.771:519.68

ABSTRACT

In the Ph.D. thesis is presented general concept of controlled stock reheating in continuous furnaces for steel industry, presented in the pusher-type furnace in ACRONI, d. o. o. Controlled stock reheating is achieved by the use of tracing reference reheating curves (RRC), where the control of stock temperature is based on real-time mathematical model of slab reheating process. RRC is defined as a function of time. Such a definition of RRC enables an exact and elegant consideration of delays. A response of furnace control system to the delay in production line is a time shift of RRC for the value of delay duration. This enables closed-loop control of the slab reheating process during normal operation as well as during delays. Efficiency and precision of furnace control during delays is the main factor for overall efficiency and energy savings of furnace operation. Delays are therefore systematically divided into five delay types. Firstly, delays are divided into those, for which the duration is not known and for those with known duration. The last are further divided on scheduled, unscheduled, delays due to different reheating times of different steel grades and delays due to synchronization with rolling mills. The last delay type enables consideration of rolling mills capacities at the reheating process in the furnace. For each delay type is determined a time shift of RRC and a prolongation of drop out interval. RRC are separately defined for different initial temperatures with a step of 50 °C. To introduce the presented furnace control system (FCS), initial RRC are imitation of stationary reheating process, which is defined by technological guidelines of the reheating in furnace. Using such a RRC for introducing FCS the material is reheated in the same way as by

primerjava rezultatov ročnega vodenja z rezultati simulacije avtomatskega vodenja. Avtomatsko vodenje omogoča za faktor 3 tesnejše sledenje končni temperaturi slabov in za faktor 2 tesnejše sledenje celotni temperaturni krivulji v primerjavi z ročnim vodenjem.

manual control. RRC can be optimized any time and the changes can be updated in the table of RRC in database. A comparison of manual and simulation of automatic control is presented at the end. Automatic control by FCS enables three times tighter tracing of end material temperature and two times tighter tracing of whole RRC in comparison to manual control.

Na Naravoslovnotehniški fakulteti Univerze v Ljubljani je dne 20. 2. 2008 pred komisijo v sestavi: red. prof. dr. Radomir Turk kot predsednik in člani: izr. prof. dr. Anton Smolej, doc. dr. Jelena Vojvodič Tuma, red. prof. dr. Franc Vodopivec, red. prof. dr. Ivan Anžel in izr. prof. dr. Boštjan Markoli, **Gorazd Kosec**, univ. dipl. inž. materialov in metalurgije zagovarjal doktorsko disertacijo z naslovom:

Krhki prelom v coni toplotnega vpliva zvarov jekla Niomol 490 K
Brittle fracture in the heat affected zone of welds of steel Niomol 490 K

Doktorska disertacija je izdelana pod mentorstvom izr. prof. dr. Antona Smoleja in somentorstvom doc. dr. Jelene Vojvodič Tuma.

KRHKI PRELOM V CONI TOPLOTNEGA VPLIVA ZVAROV JEKLA NIOMOL 490 K

UDK: 621.791.05:669.14.018.298

POVZETEK

Cilj našega dela je bil ugotoviti, zakaj je prehodna temperatura žilavosti po Charpyju zvarov tanjših plošč (15 mm) opazno višja, kot pri zvarih debelejših (25 mm) plošč jekla Niomol 490 K, čeprav je bilo varjenje opravljeno z isto tehnologijo in z enako elektrodo. Da bi našel razlago za to razliko sem pripravil z različnimi toplotnimi obdelavami jeklo različnih mikrostruktur, ki so se razlikovale tudi po velikosti kristalnih zrn. Segrevanje pri nanosu naslednjega varka sem simuliral s kratkim segrevanjem v dvofazno temperaturno področje, kjer sta obstojna avstenit in ferit. Preizkusi so obsegali merjenje žilavosti po Charpyju v razponu od popolnoma krhkega do popolnoma duktilnega preloma, meritve trdot, natezne preizkuse pri temperaturi krhkega loma ter preiskave mikrostruktur in prelomnih površin. Na podlagi eksperimentalnih rezultatov in njihove analize sklepam, da ima jeklo z mikrostrukturo iz spodnjega bainita mnogo večjo žilavost, kot jeklo z mikrostrukturo martenzita. Po ogrevanju v dvofazno področje (750 °C) se močno zmanjša žilavost pri temperaturi 0 °C in poviša prehodna temperatura žilavosti v primeru, ko je bila začetna mikrostruktura iz bainita, pri jeklu z začetno mikrostrukturo iz martenzita pa so spremembe mnogo manjše in drugačne. Vpliv pogrevanja je drugačen in mnogo manjši pri drugih lastnostih, razlaga pa je v načinu in v hitrosti obremenjevanja oz. meritve. Vpliv ogrevanja na žilavost in prehodno temperaturo je mogoče razložiti na podlagi dveh podmen, tako da pri temperaturi ogrevanja ni neposredne premene martenzita v avstenit, ampak nastane sekundarni martenzit v procesu martenzit → ferit + cementit (popuščeni martenzit) → avstenit → sekundarni martenzit, če pa je izhodni mikrostrukturi iz ferita in cementita (bainit), pa je proces, ko nastane sekundarni martenzit v naslednjih stopnjah: ferit + cementit (bainit) → avstenit → sekundarni martenzit, ter da je porazdelitev ferita in sekun-

BRITTLE FRACTURE IN THE HEAT AFFECTED ZONE OF WELDS OF STEEL NIOMOL 490 K

UDC: 621.791.05:669.14.018.298

SUMMARY

The aim of this investigation was to determine, why for the the low carbon Nb microalloyed steel Niomol 490 K and for identical welding procedure the Charpy transition temperature was higher for welds of thinner (15 mm) than for welds of thicker (25 mm) plates. With thermal treatment specimens of the steel were prepared with a different microstructure and grain size and the reheating at the next pass deposition was simulated with short time annealing in the two phase austenite + ferrite temperature of 750 °C. For all types of investigated microstructure the investigations consisted of: the determination of the dependence Charpy notch toughnes versus temperature from below the lower shelf threshold up to to 60 °C, the determination of the tensile strength by brittle fracturing and hardness; SEM examination of microstructure and of fracture surfaces and the determination of the space orientation of clevage facets of the brittle fracture.

It was found that notch toughness was much higher with lower bainite, also for the steel quenched from 1250 °C in lead bath at 400 °C, than for martensite. After reheating, the transition temperature was increased and the 20 °C notch toughness was decreased very much for bainite, while, both vere virtually unchanged for martensite. The effect of reheat is much lower for other properties.

The different effect of reheating on notch toughness can be explained assuming that:

– no direct tranformation martensite austenite takes place and secondary martensite is formed with the process: martensite → ferrite + cementite → austenite → secondary martensite, while for bainite the proces is bainite (ferrite + cementite) → austenite → secondary martensite
– and the distribution of secondary martensite and ferrite is identical or very similar to the distribution

darnega martenzita enaka, ali zelo podobna porazdelitvi ferita in cementita pred premeno v avstenit. Morfologija mikrostrukture, predvsem porazdelitev ferita in sekundarnega martenzita po ogrevanju najmočneje vplivata na žilavost in prehodno temperaturo žilavosti in to tem bolj, čim večja so bila kristalna zrna avstenita iz katere je nastala primarna mikrostruktura. Mikrostruktura ne vpliva na orientacijo oz. prostorsko lego cepilnih ploskev, ki so {110} pri izhodni primarni mikrostrukturi iz martenzita ali bainita in pri mikrostrukturah, ki so nastale z ogrevanjem le-teh.

Lokalna krhka področja (LBZ local brittle zone) zmanjšajo žilavost in povišajo prehodno temperaturo žilavosti v pasu največjih kristalnih zrn avstenita v coni toplotnega vpliva (CTV). Dokazal sem, da je premena avstenita v bainit (primarni) pri nanosu predhodnega varka mnogo bolj neugodna za žilavosti po nanosu naslednjega varka, kot če se avstenit v CTV premeni v primarni martenzit. Zato je po primarni premeni avstenita v bainit mnogo verjetneje, da bo po nanosu naslednjega varka nastala LBZ, ki bo bistveno bolj neugodna kot v primeru primarne mikrostrukture iz bainita, kot po premeni v martezit, čeprav je izhodna trdota večja pri martenzitu. Pri jeklu Niomol 490 K in njemu podobnih jeklih, se je pri varjenju izogibati premene avstenita v bainit v pasu največjih kristalnih zrn avstenita v CTV, posebej še, če lahko pri gradnji večvarkovnega vara nastanejo LBZ.

Notranje napetosti, ki so povezane z nastankom sekundarnega martenzita (LBZ) povzroče plastifikacijo matice in so največje pri temperaturi okolice. Prispevajo k nukleaciji in propagaciji razpoke pri udarnem preizkusu, pa tudi k lokalni porušitvi delcev sekundarnega martenzita (LBZ), s čimer še olajšajo nukleacijo razpoke pri udarnem preizkusu.

od ferrite and cementite before the transformation to austenite at reheating.

The distribution of ferrite and austenite before the reheating affects the notch toughness and notch transition temperature the strongest, the coarse were the austenite grain size before the formation of secondary martensite. The type of the initial and reheat microstructure does not affect the cleavage lattice plane {110}.

Local brittle zones (LBZ), which may form in the heat affected zone of welds, decrease the notch tougness and increase the transition temperature the most in the layer of coarsest austenite grain size heat affected zone. Thus, for the steel Niomol 490 K, the transformation austenite to lower bainite is more harmfull for after reheat notch toughness than the transformation austenite to primary martensite, as the microstructure of bainite is more propensive to the formation of LBZ than that of martensite, although the hardness is higher for martensite. It is consluded that by welding of the steel Niomol 490 K and similar structural steels, it is recommended to avoid the trasformation of coarse austenite to lower bainite in the coarse grained part of the heat affected zone.